INVESTIGATION OF THE STRUCTURAL, MAGNETIC AND TRANSPORT PROPERTIES OF YTTRIUM SUBSTITUTED Ni-Zn FERRITES

M.Sc. Thesis

BY

SHARMIN AKTER

DEPARTMENT OF PHYSICS

KHULNA UNIVERSITY OF ENGINEERING & TECHNOLOGY

KHULNA - 9203, BANGLADESH

FEBRUARY-2019

INVESTIGATION OF THE STRUCTURAL, MAGNETIC AND TRANSPORT PROPERTIES OF YTTRIUM SUBSTITUTED Ni-Zn FERRITES

M.Sc. Thesis

BY

SHARMIN AKTER

ROLL NO. 1755502

SESSION: JANUARY-2017

A THESIS SUBMITTED TO THE DEPARTMENT OF PHYSICS, KHULNA UNIVERSITY OF ENGINEERING & TECHNOLOGY, KHULNA - 9203 IN PARTIAL FULFILMENT OF THE REQUIREMENT FOR THE DEGREE OF MASTER OF SCIENCE

DEPARTMENT OF PHYSICS

KHULNA UNIVERSITY OF ENGINEERING & TECHNOLOGY

KHULNA - 9203, BANGLADESH

FEBRUARY - 2019

Dedicated

to

My Beloved Parents

DECLARATION

This is to certify that the thesis work entitled as **"Investigation of the Structural, Magnetic and Transport Properties of Yttrium Substituted Ni-Zn Ferrites"** has been carried out in partial fulfillment of the requirement for M.Sc. degree in the Department of Physics, Khulna University of Engineering & Technology, Khulna-9203, Bangladesh. The above research work or any part of this work has not been submitted to anywhere for the award of any degree or diploma. No other person's work has been used without due acknowledgement.

Supervisor   **Candidate**

....

Prof. Dr. Shibendra Shekher Sikder   Sharmin Akter

i

KHULNA UNIVERSITY OF ENGINEERING & TECHNOLOGY
DEPARTMENT OF PHYSICS

Approval

This is to certify that the thesis submitted by **Sharmin Akter** entitled ***"Investigation of the Structural, Magnetic and Transport Properties of Yttrium Substitated Ni-Zn Ferrites"*** has been accepted by the Board of Examiners for the partial fulfillment of the requirements for the degree of M. Sc. in the Department of Physics, Khulna University of Engineering & Technology, Khulna, Bangladesh on 20 February 2019.

Board of Examiners

Sl. No.	Name, Designation & Address	
1.	Prof. Dr. Shibendra Shekher Sikder Department of Physics Khulna University of Engineering & Technology	Chairman & Supervisor
2.	Head Department of Physics Khulna University of Engineering & Technology	Member
3.	Prof. Dr. Md. Mahbub Alam Department of Physics Khulna University of Engineering & Technology	Member
4.	Prof. Dr. Md. Abdullah Elias Akhter Department of Physics Khulna University of Engineering & Technology	Member
5.	Dr. Mohammed Nazrul Islam Khan Principal Scientific Officer Material Science Division Atomic Energy Center, Dhaka-1000.	Member (External)

Acknowledgements

ABSTRACT

The present research work is focused on Yttrium (Y) doped Ni-Zn ferrites. The ferrite samples of the composition $Ni_{0.25}Zn_{0.75}Y_xFe_{2-x}O_4$ [where x= 0.00, 0.02, 0.04, 0.06 and 0.08] were synthesized by conventional solid state reaction method. As a part of synthesis the samples were pre-sintered at 850°C for 2 hours and sintered at 1150°C for 3 hours. The effect of rare earth Y^{3+} substitution on the structural, magnetic and electrical properties of the Ni-Zn ferrites was studied. The phase identification and lattice parameter determination were carried out by using X-ray diffraction (XRD). XRD patterns show that all the samples consisted of the single phase cubic spinel structure with an extra peak in x=0.08**.** The lattice parameters gradually increases with increasing Y content but it slightly decreased for x=0.08. The bulk density suddenly decrease for x=0.02 then increases with increasing rare earth Y^{3+} ion and again slightly decreased for x=0.08. The X-ray density increases continuously with increasing x-content. The microstructural analysis was done by Scanning Electron Microscopy (SEM). The SEM images show that the samples exhibit uniform surface morphology with well-defined spherical grains. The average grain size was calculated using Image J software and it can be observed that the average grain size gradually increased with Y content except x=0.08 where it decreases suddenly. The complex permeability, loss tangent and dielectric properties were investigated as a function of frequency range 1 KHz to 120 MHz by using an impedance analyzer. The initial permeability was found in steady state to a higher order of frequency range from 10^3 Hz - 50 MHz. Continuous decrease of the dielectric constant with the increasing frequency and remains almost constant at higher frequency range has been observed. The magnetic properties have been studied by Vibrating Sample Magnetometer (VSM). The saturation magnetization(M_s), coercivity(H_c), remanent magnetization(M_r) and the ratio of remanent magnetization and saturation magnetization have been calculated from the M-H loop at room temperature. The values of M_s were decreases with increasing Y^{3+} content. Moreover, coercivity decreases with increasing Y content. Doping of Y ion lowers the conduction and subsequently an increase in resistivity is observed. The characteristics of electromagnetism, excellent chemical stability, mechanical hardness, high coercivity, and moderate saturation magnetization have made Y doped Ni-Zn ferrite a good candidate for synthesizing and investigation to contribute in science and technology.

Contents

CHAPTER - I
INTRODUCTION

CHAPTER - II
THEROETICAL BACKGROUND

CHAPTER-III

EXPERIMENTAL PROCEDURE

CHAPTER-IV
RESULTS AND   DISCUSSION

CHAPTER-V
CONCLUSIONS

List of Figures

List of Tables

List of Symbols

XRD	=	X-Ray Diffraction
VSM	=	Vibrating Sample Magnetometer
SEM	=	Scanning Electron Microscopy
DC	=	Direct Current
RE	=	Rare Earth
FCC	=	Face Centered Cubic
T_N	=	Nell Temperature
ρ_B	=	Bulk density
ρ_x	=	X-ray density
ρ_{DC}	=	DC Resistivity
M_S	=	Saturation magnetization
M_r	=	Remanent magnetization
K_u	=	Anisotropy constant
H_c	=	Coercive force
μ_B	=	Magnetic moment in Bohr magneton.
μ	=	Permeability
μ'	=	Real part of the complex permeability
μ''	=	imaginary part of the complex permeability
ε	=	Dielectric constant
ε'	=	Real part of the dielectric constant
ε''	=	imaginary part of the complex permeability
D	=	Grain size
Φ	=	Magnetic Flux
I	=	Intensity of Magnetization
B	=	Magnetic induction
H	=	Magnetic field
a	=	Lattice parameter
$\tan \delta$	=	loss factor or loss tangent
λ	=	Wave length of the X-ray
[hkl]	=	Miller Indices of a peak
δ	=	Phase Angle

R	=	Resistance
T	=	Torque
B	=	External Magnetic Field
I	=	Intensity of Magnetization
χ	=	Magnetic Susceptibility
C	=	Capacitance of a Capacitor
C_o	=	Capacitance of a Capacitor with Vacuum
$F(\theta)$	=	Nelson Riley Function
Q	=	Quality Factor
RQF	=	Relative Quality Factor

CHAPTER I

Introduction

INTRODUCTION

1.1   Introduction

The term ferrite denotes a group of iron oxides, which have the general formula MO. Fe_2O_4, where, M is a divalent metal ion such as Mn^{2+}, Fe^{2+}, Co^{2+}, Ni^{2+}, Cu^{2+}, Zn^{2+}, Mg^{2+} or Cd^{2+}. Recently rare earths (RE) substituted different ferrites are becoming the promising materials for different applications for engineering magnetic materials. Addition of small amount of RE ions to ferrite samples produces a change in their magnetic, transport as well as structural properties depending upon the type of electrical component and the amount of RE elements used. Ferrimagnetism in ferrite is largely governed by Fe-Fe interaction spin coupling of the 3d electrons. The RE ions form enter the spinel lattice, the RE-Fe interactions also appears 4f-3d coupling, which can lead to change in the magnetization and Curie temperature. The RE-RE interactions are very weak since the result from the indirect 4f-5d-5d-4f mechanism.

Ferrites are used in power electronic device from the radio frequency used in between 300kHz to 3MHz and microwave frequency between 3MHz to 20GHz used in bubble devices, audio, video and digital recording and as permanent magnets [Von Aulock, 1965; Shah, 1971; Senelling, 1988; Van Vleck, 1989; Spaldin, 2003]. Today Ni-Zn ferrites are one of the most versatile, reasonable cost magnetic materials for general use in both low and high frequency devices because of their high resistivity, low dielectric losses, mechanically hardness, high Curie temperature and chemical stability [Ahmed *et al.,* 2003; Hossain *et al.,* 2017]. Ni-Zn ferrites are used in radiofrequency circuits, microwave devices, magnetic fluids, transformer cores, read\write heads for high-speed digital tapes, operating devices. Ferrites are ferromagnetic substance with spinel structure able to form an extremely wide variety of solid solutions.

Spinel ferrite is one of the most important classes of magnetic ceramic materials owing interesting applications. This means that the composition of a given ferrite can be strongly modified, while the basic crystalline structure remains the same. It has tetrahedral A-site and octahedral B-site in AB_2O_4 crystal structure. Depending on A- and B-site cations it can exhibit ferromagnetic, antiferromagnetic, ferrimagnetic, spin (cluster) glass, and paramagnetic behaviors [Gupta and Coble, 1968; Kigery *et al.,* 1975; Lange, 1989]. Various cations can be placed in A- and B-site to tune its magnetic properties. This distribution is

different when the ferrite is synthesized at low temperature [Tsay *et al.,* 2000]. Spinel ferrites are prepared through various methods like solid state reaction method, high energy ball milling method, sol-gel method, chemical co-precipitation method, microwave sintering method, auto combustion method, conventional ceramic technique, conventional two-step synthesis method etc. Here we have used solid state reaction method. In this method, different metal oxides are mixed and calcined to get ferrite powders.

However, mechanical mixing of different oxides is hardly intimate and homogeneous and hence it results in composition fluctuation at every stage of processing that also persists after sintering [Paulus *et al.,* 1978]. High values of electrical resistivity can be attained by doping these ferrites with proper divalent cations, as well as by controlling their microstructure. It is mentioned that ultra fine grains would provide a large number grain boundaries which may act as a barrier for electron flow, resulting in the reduction of eddy current losses [Verma *et al.,* 1948].

Properties of the ferrites are highly sensitive to the ferrite compositions and synthesis techniques [Li *et al.,* 2012]. At present, a large amount of work has been done to investigate its electromagnetic properties by changing the method of preparation (such as solid-state reaction method, sol–gel method, organic acid precursor method and molten-salt synthesis), chemical composition, additive, sintering temperature, time, etc. [Herzer *et al.,* 2005]. The interest in the wet m-chemical synthesis of ultra fine ferrite powders enabling production of ferrites with high density at low temperatures is demandable. Solid state reaction method technique meets the increasing demand for preparation of these powders.

This work has investigated that effect of RE ion substituted for the Fe ion in a Ni-Zn ferrite on the magnetic, structural and transport properties. The structural, magnetic and electrical properties of these ferrites depend on the relative distribution of cations at the different sites as well as the preparation condition. Ni-Zn ferrites are mixed spinel in which the tetrahedral (A) sites are occupied by Zn^{2+} and Fe^{3+} ions and the octahedral sites (B) are occupied by Ni^{2+} and Fe^{3+} ions in the spinel formula AB_2O_4.The magnetic and dielectric properties depend on this distribution of these ions on tetrahedral and octahedral sites. Because RE atoms in Ni-Zn ferrites play an important role in determining the magneto crystalline anisotropy in the 4f-3d intermetallic compounds. In this work, we reported the structural and magnetic properties Ni-Zn ferrites in the influence of Yttrium (Y^{3+})

substitution on the microwave absorption properties. The effect of substitutions with rare-earth (Y^{3+}) on Ni-Zn ferrites has been found that the octahedral sides (B) of rare-earth Y^{3+} ions prevents the motion of Fe^{2+} in the conduction process, thus causing an increase in resistivity. By optimally choosing the substitutions, it is possible to obtain a good soft magnetic material.

1.2   The Aims and Objectives of Recent Work

Scientists still continue their efforts to find out optimum parameters of ferrites, like high saturation magnetization, high permeability and high resistivity. Till now researchers have not yet been able to formulate a rigid set of rules for ferrites about a single property. The addition of rare earth metal Y^{3+} ions in Ni-Zn ferrite composition should be maintained in such way so that prepared ferrite materials ensure high permeability and their high resistivity as a prime requisite for good inductor material. Ferrites are also especially convenient for high frequency uses because of their high resistivity. The high frequency response of the complex permeability is therefore very useful in determining the convenient frequency range in which a particular ferrite material can be used. The mechanism of eddy current losses and damping of domain wall motion can be understood from the relative magnitudes of the real and imaginary parts of the complex permeability. The effect of composition and microstructure on the frequency response is therefore very useful.
The main objectives of the present research are as follows:

- Preparation of various $Ni_{0.25}Zn_{0.75}Y_xFe_{2-x}O_4$ [Where x = 0.00, 0.02, 0.04, 0.06 and 0.08] samples by solid state reaction technique.
- Determination of crystal structure (X-ray diffraction), density and porosity of Ni-Zn ferrite.
- Optimize the concentration of rare earth Y doped for the best magnetic and transport properties.
- To study structural, electrical, transport and magnetic properties of all the prepared samples such as: Magnetization, Magnetic loss components, Permeability, Resistivity, Dielectric constant and Microstructure.

Finally, it is expected to use powder particles as starting materials may give uniform microstructure exhibiting better magnetic and electrical transport properties. With the

substitution of rare earth metals Y in the Ni-Zn ferrite system permeability and magnetic properties are expected to be improved. Thus this system will have further good technological application in high frequency range. In our research in soft magnetic materials and in rare earth metal doped ferrites, Bangladesh may develop a profitable electronic industry.

1.3   Experimental Reason for This Research Work

Rare earth Y doped Ni-Zn ferrites sample have been prepared by conventional solid state reaction technique using high purity oxide nanomaterials. High purity powder of Ni_2O_3 (99.99%), ZnO (99.99%), Y_2O_3 (99.99) and Fe_2O_3 (99.99), are mixed thoroughly in an appropriate amount. Mixing have been performed in both dry and acetone media. The mixed powders have been calcined at high temperature. After calcination toroid and disk shape samples are sintered at various temperatures. The experimental that have been used in this research work are as follows:

- Sintering of the samples will be carried out in a microprocessor controlled high temperature furnace department of Physics, Khulna University of Engineering & Technology (KUET), Khulna.

- The prepared sample would be characterized in terms of their crystal structure, unit cell parameters and phase presents in the prepared sample with the help of X-ray diffractometer (XRD) in the material science division, Bangladesh Atomic Energy Center (BAEC), Dhaka The porosity of the prepared samples have been calculated from the theoretical density (using XRD data).

- Surface morphology of the samples will be investigated using a Scanning Electron Microscope in the material science division, Bangladesh Atomic Energy Center (BAEC), Dhaka.

- Permeability, magnetic loss factor and quality factor as function of frequency have been determining using impedance analyzer in the department of Physics, Khulna University of Engineering & Technology (KUET), Khulna.

- Magnetizations of the samples have been measured as a function of field using vibrating sample magnetometer (VSM) in the material science division, Bangladesh Atomic Energy Center (BAEC), Dhaka.

- Dielectric properties as a function of frequency have been studied with the help of inductance meter department of Physics, Khulna University of Engineering & Technology (KUET), Khulna.

- DC electrical resistivity as a function temperature has been studied with the help Magnetizations of electrometer in the department of Physics, Khulna University of Engineering & Technology (KUET), Khulna.

1.4 Ferrites and their importance

Ferrites are very important magnetic materials especially rare earth doped because of their first attracted the attention was their negligible electrical eddy current losses that make in ferrites indispensable materials in telecommunications and in the electronic industry. Saturation magnetization (M_S), coercive force (H_C) and initial permeability (μ_i) are the most important parameters for the good quality presentation in application and secret by the initial permeability, for the low and high frequency applications. Ferrites are used widely due to their following application.

(i)   Ferrites are part of low power and high flux transformers which are used in television.

(ii)   Small antennas are made by winding a coil on ferrite rod used in transistor radio receiver.

(iii) Soft ferrites were used for the manufacture of inductor core in combination with capacitor circuits in telephone system, but now a day solid state devices have replaced them. The soft Ni-Zn and Mn-Zn ferrites are used for core manufacture.

(iv)   In computer, non volatile memories are made of ferrite materials. They store information even if power supply fails. Non-volatile memories are made up of ferrite materials as they are highly stable against severe shock and vibrations.

(v)   Ferrites are used in microwave devices like circulators, isolators, switch phase shifters and in radar circuits.

(vi)   Ferrites are used in high frequency transformer core and computer memories i.e. computer hard disk, floppy disks, credit cards, audio cassettes, video cassettes and recorder heads.

(vii)   Ferrites are used to produce low frequency ultrasonic waves by magnetostriction.

(viii)   Nickel alloys are used in high frequency equipments like high speed relays, wideband transformers and inductors. They are used to manufacture transformers, inductors, small motors, synchros and relays. They are used for precision voltage and current transformers and inductive potentiometers.

(ix)   They are used as electromagnetic wave absorbers at low dielectric values.

(x)   Ferrites are important components for the latest products, such as cellular phones, video cameras, note book computers, hard temperatures and floppy drives.

(xi)   Ferrites for the applications in producing multilayer-type chips mainly because these oxides can be sintered at relatively low with a wide range of compositions.

(xii)   There are several Japanese installations which use precipitation of ferrite precursors for searching pollutant materials such as mercury from waste streams. The ferrites formed subsequently can be alienated magnetically along with the pollutant.

(xiii)   As ferrites have high corrosion resistance, therefore, having the appropriate conductivities they can be used as electrode in applications mainly in chromium plating.

1.5   Background of Material Selection: Literature Review

Spinel ferrites are extremely important for academic and technological interest. The structural, electrical and magnetic properties are governed by the type of magnetic ions residing on the A site and B-site of the spinel lattice and the relative strength of inter and intra sub lattice interactions. Magnetic properties of Ni-Zn ferrite nanoparticles have been studied by Lu *et al.,* 2011. The saturation magnetization has high about 55 emu/gm and comparable to the reported value of high temperatures sintered Ni-Zn ferrite. The XRD patterns have confirmed the single phase spinel structure. In this research, the proposed sample has the formula of $Ni_{0.25}Zn_{0.75}Y_xFe_{2-x}O_4$ [where x=0.00, 0.02, 0.04, 0.06, 0.08]. Now

the reason of Ni-Zn ferrite selection has been attributed by studying common problems with Ni-Zn ferrites. The literatures are given here:

Guo *et al.,* [2010] synthesized the structural and magnetic properties of Ni-Zn ferrite films with high saturation magnetization. They observed the XRD patterns and confirm the samples were well crystallized and single phase. SEM images indicated that all the samples consisted of particles nanocrystaline in nature. They have observed a large real part of permeability, μ_i a very high resonance frequency f_r of 1.2 GHz. Naughton *et al.,* [2007] investigated by lattice parameter and saturation magnetization of Ni-Zn ferrites. The lower saturation magnetization was attributed to a combination of the large lattice parameter decreasing the per-exchange interactions between the Ni^{2+} and Fe^{3+} ions and incomplete ordering of the cations between the octahedral and tetrahedral sites in the spinel structure.

Abdeen [1998] studied electric conduction in Ni-Zn ferrite. The real AC and DC electrical conductivities increase as the temperature increases indicating the studied samples are semiconductors in nature. The AC electrical conductivity increases with increasing angular frequency below T_C and above T_C it is independent of nature. The values of T_C decrease with increasing Zn content and activation energy below and above T_C decreases with increasing Zn-content.

Khan *et al.,* [2013] reported that Ni-Cu-Zn ferrites are well established soft magnetic materials for MLCI application because of their relatively low sintering temperature, high permeability in the rf-frequency region and high electrical resistivity. Khan *et al*., [2013] studied complex permeability spectra of Ni-Cu-Zn ferrites. The particle size increase with increasing the sintering temperature and it was also found that the real part of initial permeability of the low frequency region decreases.

Nakamura [1997] reported on frequency dispersion of permeability in ferrite composite materials. The permeability increases with increasing density of composite materials. As the ferrite content decreases both the real and imaginary parts of the low frequency permeability is significantly reduced, and the peak frequency of imaginary part of permeability shifts toward higher frequency. Nakamura *et al.,* [1994] reported on low temperature sintering Ni-Cu-Zn ferrite and its permeability spectra. The post sintering density and the complex permeability Ni-Cu-Zn ferrite ceramic can be controlled by altering the particle size of the sintering oxide materials and calcinations temperature.

Haque *et al.,* [2013] reported the magnetic properties of $Mg_{1-x}Zn_x Fe_2O_4$ ferrites prepared by solid state reaction method. They observed that the lattice parameter increases linearly with the increase in Zn content. The Curie temperature (T_c) decreases with increase in Zn content. The μ_i increases with the addition of Zn^{2+} ions but the resonance frequency shift towards the lower frequency.

Ahmed *et al.,* [2017] reported the effect of rare earth ions on the structural, magnetic and electrical properties of $(Mn_{0.5} Zn_{0.5})RE_{0.05} Fe_{1.95}O_4$ ferrites where RE = Tb, La, Ce, and Th. Rare earth ions formed orthoferrite ($REFeO_3$) phase and formation of these secondary phase in ferrite during sintering process was governed by the type and the amount of RE^{3+} in used. It was found that the molar magnetic susceptibility for rare earth substituted samples were smaller than pure ferrite. T_c and electrical resistivity increased with increasing rare earth ions in Mn-Zn ferrites.

Jacobo *et al.,* [2004] investigated by the impact of Y^{3+} concentration on the magnetic and microwave absorption properties of $Ni_{0.05}Zn_{0.05}Y_xFe_{2-x}O_4$ ($0.01 \leq x \leq 0.05$) nano ferrites was Crystallite sizes and cell parameters decreased with increase in Y substitution and it also modified the saturation magnetization, permeability, and permittivity in the explored frequency range. The variation in the dielectric constant has also been discussed with the increase in yttrium concentration. The maximum of the magnetic losses diminishes and shifts to higher frequencies with yttrium inclusion. Yttrium-doped Ni–Zn ferrites (with Y content ≤ 0.05 per formula unit) can be considered good attenuators in the explored high- frequency microwave range.

Jacobo *et al.,* [2011] worked on ($Zn_{0.5}Ni_{0.5}RE_{0.02}Fe_{1.98}O_4$) ferrites, with RE = Y, Gd and Eu. The results showed a small increase in the hyperfine field parameters and a strong decrease of the total resonant area with respect to the pure Ni-Zn ferrite. Curie temperatures decreased and coercive fields increased with substitution rare earth ions. By adding much large ionic radii rare earth ions resulted in local distortion and disorder, enough to induce a softening of the network electron density.

Sun *et al.,* [2004] investigated the effects of rare earth ions on the properties of $(Ni_{0.5}Zn_{0.5})Fe_{1.98}RE_{0.02}O_4$ (RE = Y, Eu or Gd) nominal compositions. The partial substitution of Fe^{3+} with a small amount of RE ions increased the electrical resistivity and relative loss factor, whereas, it slightly decreased the T_c. Rezlescu *et al.,* [1994] investigated the influence

of rare earth ions like Yb, Er, Dy, Tb, Gd, Sm substitution on structure, magnetic and electrical properties of $(Li_{0.3}Zn_{0.4})Fe_{1.96}RE_{0.04}O_4$ ferrites. They found that RE_2O_3 facilities the formation of secondary phases at grain boundary which suppressed the grain growth and results are showed that the T_c shifted to lower temperature and increased the electrical resistivity.

From the above mentioned review is observed that physical, magnetic, electrical transport and microstructural properties are strongly dependent rare earth substitutions Ni-Zn ferrites in a very complicated way and there is no straight forward relationship between the nature and the quantity of doping on several factors like sintering conditions, preparation methods, compositions etc. High permeability attainment is certainly affected by the microstructure of the ferrites. The very high permeability is restricted to certain temperature ranges and the shapes of permeability versus temperature curves are strongly affected by any inhomogeneity in the ferrite structure.

In the present work, the attempt is made to systematically investigate the structural, magnetic, electric and dielectric properties of rare earth (RE = Y^{3+}, x =0.00, 0.02, 0.04, 0.06 and 0.08) substituted $Ni_{0.25}Zn_{0.75}Y_xFe_{2-x}O_4$ spinel ferrites and it is prepared by Solid State Reaction Method. Nonmagnetic Zn^{2+} ion is very promising and interesting substitution to handle the electromagnetic properties of ferrite materials.

1.6 Outline of the Thesis

The thesis has been configured into five chapters which are as follows:

Chapter 1: Introduction

In this chapter, presents a brief introduction to Y doped Ni-Zn ferrites and organization of thesis. This chapter incorporates background information to assist in understanding the aims and objectives of this investigation, and also reviews recent reports by other investigators with which these results can compared.

Chapter 2: Theoretical Background

In this chapter, a briefly describe theories necessary to understand magnetic materials as well as ferrites, classification of ferrites, cation distribution, super exchange interaction, two sub lattices modules etc. have been discussed in details.

Chapter 3: Experimental Background

In this chapter, the experiment procedures are briefly explained along with description of the sample preparation, raw materials. This chapter deals with mainly the design and construction of experimental and preparation of ferrite samples. The fundamentals and working principles of measurement set up are discussed.

Chapter 4: Results and Discussion

In this chapter, results and discussion are thoroughly explained. The various experimental and theoretical studies namely Effect of Rare Earth Metal Substitution on the Structural, Electrical and Magnetic properties of Y doped Ni-Zn Ferrites are presented and discussed step by step.

Chapter 5: Conclusion

In this chapter, the results obtained in this study are summarized. Suggestions for future works on these studies are included. Finally, a complete list of references and publications has been given towards the end of this chapter.

CHAPTER II

THEROETICAL BACKGROUND

THEROETICAL BACKGROUND

2.1   Rare Earth Ferrites

The rare earth substituted different ferrites are becoming the promising materials for different applications. Addition of small amount of rare earth ions to ferrite samples producing a change in their magnetic and electrical as well as structural properties depending upon the types and the amount of rare earth elements used. Rare earth elements are a group of seventeen chemical elements that occur together in the periodic table. The group consists of yttrium and the 16 lanthanide elements are lanthanum, cerium, praseodymium, neodymium, promethium, samarium, europium, gadolinium, terbium, dysprosium, holmium, erbium, thulium, ytterbium, scandium and lutetium. They are also referred to as "rare earth oxides" because many of them are typically sold as oxide compounds. Rare earth elements are not as "rare" as their name implies. Thulium and lutetium are the two least abundant rare earth elements - but they each have an average crustal abundance that is nearly 200 times greater than the crustal abundance of gold [Rare Earth Elements]. However, these metals are very difficult to mine because it is unusual to find them in concentrations high enough for economical extraction.

The better properties of ferrites can be achieved through proper doping of rare earth metals and recently rare earth (RE) doped ferrites become interesting due to their superiority for various applications such as structural, magnetic and electrical properties over other doped ferrite systems [Bharathi *et al.*, 2009; Peng *et al.*, 2011; Guo *et al.*, 2010; Nikumbh *et al.*, 2014]. The

11

rare earth ions can be divided into two categories; one with the radius closes to Fe ions; while the other with ionic radius larger than Fe ions [Rezlescu *et al.*, 1994]. The difference in their ionic radii will lead to micro strains, which may cause domain wall motion resulting in deformation of the spinel structure. It has been stated that ions commonly reside at the octahedral sites by replacing Fe^{3+} ions and have limited solubility in the spinel lattices due to their large ionic radii [Naughton *et al.*, 2007]. The lower saturation magnetization was attributed to a combination of the large lattice parameter, decreasing the per-exchange interactions between the Ni^{2+} and Fe^{2+} ions and incomplete ordering of the cations between the octahedral and tetrahedral sites in the spinel structure. The rare earth ions have unpaired 4f electrons and the strong spin orbit coupling of the angular momentum. 4f shell of RE ions is shielded by $5S^2 5P^6$ and almost not affected by the potential field of surrounding ions. Doping rare earth ions into spinel type ferrites, the occurrence of 4f-3d couplings which determine the magneto-crystalline anisotropy in spinel ferrite can also improve the electric and magnetic properties of spinel ferrites [Jing *et al.*, 2006; Jing *et al.*, 2007; Vanuuitert, 1955; Kolekar *et al.*, 1995].

Spinel ferrites ceramic are widely used in microwave devices to control transmission path, frequency, amplitude and phase of microwave signals. Accurate dielectric and magnetic properties measurement at the operational frequency and temperature ranges are needed for optimized development of these devices, as well as to assist in the manufacture of the ferrite [Jie *et al.*, 2010]. The magnetic properties of RE ions have wide variations: (i) their magnetic moment varies from 0 (La^{3+}) to 10.6 μ_B (Dy^{3+}) and (ii) they can be isotropic or anisotropic in relation with the variation in the f electron orbital contribution to magnetic interactions [Kambale *et al.*, 2011]. The properties of ferrites are being improved due to the increasing trends in ferrite technology. It is believed that there is a bright future for ferrite technology. Ferrimagnetisms in ferrite is largely governed by Fe-Fe interaction, i.e. the spin coupling of the 3d electron. If the rare earth ions the spinel lattice, the RE-Fe interactions also appears 4f-3d coupling, which can lead to changes in the specific magnetization and Curie temperature. The great interest of Y doped Ni-Zn ferrites, both their technological applications and theoretical understanding of the mechanisms involved, the present research is aimed at finding the Y ions.

2.2   Brief History of Ferrimagnetism and Ferrites

Ferrimagnetism is exhibited by ferrites and magnetic garnets. The oldest known magnetic substance, magnetites like Fe^{2+} and Fe^{3+} oxide; Fe_3O_4, is a ferrimagnet; it was originally classified as a ferrimagnet before Neel's discovery of ferrimagnetism and antiferromagnetism [Néel, 1948]. A ferrimagnetic material is one that has populations of atoms with opposing magnetic moment, as in ferromagnetism; however, in ferrimagnetic materials, the opposing moments are unequal and a spontaneous magnetism remains [Spladin and Nicola, 2010]. This happens when the populations consist of different materials or ions such as Fe^{2+} and Fe^{3+}. The ferrimagnetic material does not lose its magnetism even in the absence of external magnetic field. In ferromagnetic materials, the magnetic structure is composed of two magnetic sublattices are A and B separated by oxygen's. The exchange interactions are mediated by the oxygen anions. When this happens, the interactions are called indirect or superexchange interactions. The strongest superexchange interactions result in an antiparallel alignment of spins between the A and B sublattice. The magnetic moments of the A and B sublattices are not equal and result in a net magnetic moment. Ferrimagnetism is therefore similar to ferromagnetism. It exhibits all the hallmarks of ferromagnetic behavior- spontaneous magnetization, Curie temperatures, hysteresis, and remanence.
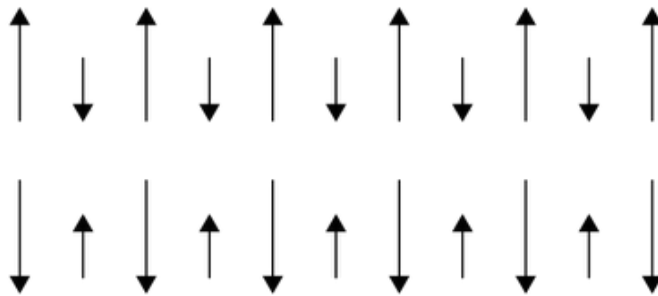
Figure 2.1: Ferrimagnetism

Double oxides of iron and other metals are important members of ferrimagnetic system commonly known as ferrites. The outstanding properties of ferrites are their complex magnetic structure, which can be varied to tailor their magnetic properties for various high frequency applications. Ferrites exhibit dielectric properties. Exhibiting dielectric properties means that even through electromagnetic waves can pass through ferrites, they do not readily conduct electricity. This also gives them an advantage over irons, nickel and other transition metals that have magnetic properties in many applications because these metals conduct electricity. Another

important factor which is of considerable importance in ferrites and is completely insignificant in metals is the porosity. Such a considerable helps us to explain why ferrites have been used and studied for several years.

Ferrites are essentially ceramic materials, compound of iron, boron, barium strontium, lead, zinc, magnesium or manganese. The ingredients are mixed, prefired, milled / crushed, dried, shaped and finally pressed and fired into their final hand in brittle state. Ferrites are a class of chemical compounds with the formula AB_2O_4, where A and B represent various metal cations usually including iron. These ceramic materials are used in applications ranging from magnetic components in micro electronics. At high frequencies ferrites are considered superior to other magnetic materials because they have low eddy current losses and high DC electrical resistibility. Ferrites are electrically non-conductive ferrimagnetic ceramic compound materials, consisting of various mixtures of iron oxides such as Hematite (Fe_2O_3) or Magnetite (Fe_3O_4) and the oxides of other metals like NiO, CuO, ZnO, MnO, CoO. They are both electrically nonconductive and ferrimagnetic, meaning they can be magnetized or attracted to a magnet. On the other hand ferrites are a class of ferrimagnetic ceramic chemical compounds consists of mixtures of various metallic oxides including Fe_2O_3 and are used in applications ranging from magnetic components in microelectronics.

2.3   Types of Ferrites

According to crystallographic structures ferrites can be classified into three different types [Standley, 1972]:

      (i)   Spinel ferrites (Cubic ferrites)

      (ii)   Hexagonal ferrites

      (iii)   Garnets

Our research work is on spinel ferrites; therefore we will discuss in detail the spinel ferrites others will be briefly discussed.

2.3.1 Spinel Structure of Ferrites

The spinel ferrites are a large group of oxides which possess the structure of the mineral spinel $MgAl_2O_4$. Spinels are basically predominantly ionic. The particular sites occupied by cations are influenced by several factors, including covalent bonding affects for example Zn in

tetrahedral sites. Many different cation combinations may form a spinel structure to combine any three cations with a total charge of eight to balance the charge of the anions [Buschow and De Boer, 2004]. The chemical composition of a spinel ferrite from the magnetic point of view are the MFe_2O_4 where M is a divalent metal ion such as Co^{2+}, Zn^{2+}, Fe^{2+}, Mg^{2+}, Ni^{2+}, Cd^{2+}, Cu^{2+} or a combination of these ions [Valenzuela, 1994].

The unit cell of spinel ferrite is fcc with eight formula units per unit cell. The formula can be written as $M_8Fe_{16}O_{32}$. The anions are the greatest and they form an fcc lattice. Within these lattices two types of interstitial positions occur and these are occupied by the metallic cations. There are 96 interstitial sites in the unit cell, 64 tetrahedral (A) and 32 octahedral (B) sites. The sites are so narrow because they are surrounded by four and six ions at equal distances respectively. The lattice characteristics of a spinel includes a face centre cubic (fcc) site for two oxygen atoms and two cationic sites occupying A and B sites in a spinel [Livingston, 1996; Culity, 1972]. Thus the unit cell contains 8 formula units AB_2O_4 with 8sites, 16 B sites and 32 oxygen ions, and total of 56 ions. A spinel unit cell contains two subcels shown in Figure 2.2. These two types of subcells alternate in a three dimensional array so that each fully repeating unit cell require 8 subcells.
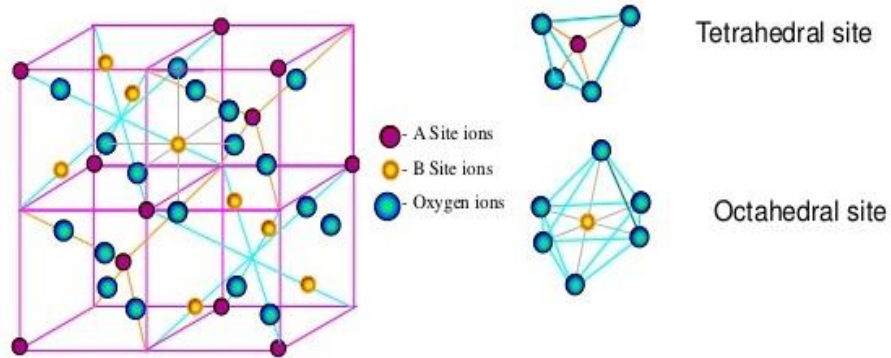
Figure 2.2: Crystal Structure of spinel ferrite

The positions of the ions in the spinel lattice are not perfectly regular as the packing of hard spheres and some distortion does occur. The tetrahedral sites are often too small for the metal ions so that the oxygen ions move slightly to accommodate them. The oxygen ions connected with the octahedral sites move in such a way as to shrink the size the octahedral cell by the same

amount as the tetrahedral site expands. The movement of the tetrahedral oxygen is reflected in a quantity called the oxygen parameter, which is the distance between the oxygen ion and the face of the cube edge along the cube diagonal of the spinel subcell.

➢ **Octahedral Site**

    (i)   16 B-sites demonstrates octahedral site

    (ii) An interstitial atom at the space in the interstices between 6 atoms forming regular octahedron.

    (iii) Four regular atoms are positioned in a single plane; the remaining two are located at symmetrical positions just above or below.

➢ **Tetrahedral Site**

    (i)   8 A-sites metal ions in tetrahedral site coordination with oxygen,

    (ii) Tetrahedral site, the interstitial is at the center of a tetrahedron formed by the four lattice atoms.

    (iii) Three adjacent atoms are in a plane; the fourth atom is located at the top symmetrical position.

    (iv) The tetrahedral site defined geometry provides a space for an interstitial atom

The factors affecting the cation distribution over A- and B-sites are as follows [Alex Goldman, 1990; Craik, 1975]:

    • Ionic size of cations

    • Electromagnetic configuration of the cations

    • Electronic energy

Smaller cations prefer to occupy the A-sites. The cations have special preference for A and B-sites and the preference depend upon the following factors:

    • Ionic radius

    • Size of interstices

    • Temperature

    • Orbital preference for the specific coordination.

The preference of cations is according to Verway- Heilmar scheme [Verway *et al.,* 1947]

    (i)   Ions with strong preference for A-sites Zn^{2+}, Cd^{2+}, Ga^{2+}, In^{3+}, Ge^{4+}.

    (ii)   Ions with strong preference for B-sites Ni^{2+}, Cr^{3+}, Ti^{4+}, Sn^{4+}.

(iii)   Indifferent ions are Mg^{2+}, Al^{3+}, Fe^{2+}, Co^{2+}, Mn^{2+}, Fe^{3+}, Cu^{2+}.

Moreover the electrostatic energy also affects the cation distribution in the spinel lattice.

2.3.2 Hexagonal Ferrites

Hexaferrites are hexagonal or rhombohedral ferromagnetic oxides with formula $MFe_{12}O_{19}$, where M is an element like Barium, Lead or Strontium. The third type o ferrites are often called the barium ferrites. These compound usually cation BaO, in addition to Fe_2O_3, as the basic component oxide. They are also known as magneto plumbites. The common chemical formula of barium ferrites is l $(BaO).m$ $(MO).N$ $(Fe_2O_3)_n$ or $Ba^{3+}.Mm^{2+}Fe_{2n}^{3+}O^{2-}_{l+m+3n}$, where l is much more complex than the previous two in both in terms of composition of barium ferrites may be complex than the previous two in both in terms of composition of barium ferrites may be changed one is to vary the M^{3+}ions. Mg, Mn, Fe, Co, Ni, Cu and Zn are found suitable for the formation of hexagonal ferrites. Another way to alter the values of l, m and n. Basic compositions are found at 1-0-6(M), 1-2-8 (M_2W), 2-2-6 (M_2Y) and 3-2-12$(M_2$). In these ferrites, oxygen ions have closed packed hexagonal crystal structure. They are widely used as permanent magnets and have high coercivity. They are used at very high frequency. Their hexagonal ferrite lattices are similar to the spinel structure with closely packed oxygen ions, but there are also metal ions at some layers with the same ionic radii as that of oxygen ions. Hexagonal ferrites have larger ions than that of garnet ferrite and are formed by the replacement of oxygen ions. Most of these larger ions are barium, strontium or lead.

2.3.3 Garnets

The mineral garnet refers to group of mixed oxides, of which the widely known on has the chemical formula $Mn_3Al_2Si_{13}O_{12}$, or equivalently $3MnO. Al_2O_3.3Si_2O_3$ single magnetic garnets have the general formula.

$$3M_2O_3. 5 Fe_2O_3 = 2 M_3^{3+}Fe_5^{3+}O_{12}$$
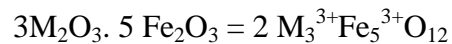
It is to be noted that in magnetic garnets the 24 positive charge units per formula units are divided unequally between the ferrites ions (15 units) and another species of trivalent ions (9 units). Technically metal garnets are those with M = Sm, Eu, Gd, Tb, Dy, Ho, Er, Tm, Yb and Yttrium. They are known as rare garnets. A code system has been adopted to name them. REG stands for the rare earth garnets, GDIG for gadolinium-iron garnet ($Gd_3 Fe_5O_{12}$) etc. Garnets

crystallize in the cubic system with two fifths of the ferrite ions forming a bcc lattice, like ferrospinels, the garnets too. Pach a large number (160) of ions in eight units formula unit cell. The lattice constant is nearly 12.5^0A about 50% larger than those ferrospinel. Also the crystal structure of garnets is more complicated than the spinel structure because of the size $(0.85-1.10^0$ A) of the M^{3+} ions. They are too large to be accommodated at the interstitial sites between the oxygen ions. Hence the oxygen ions are prohibited from forming a close packed structure as in the spinel. The general formulas for the unit cell of a pure iron garnet have eight formula units of $M_3Fe_5O_{12}$, where M is trivalent rare earth ions (Y, Gd, Dy). Their cell shape is cubic and the edge length is about 12.5^0A. They have complex crystal structures. They are important due to their application in memory structure. Garnets can be quite useful materials in microwave applications because of their high electrical resistivity and hence lower losses around microwave frequencies. Garnet material is also easy to synesize in either of bulk polycrystalline ceramic, single crystal or thin film forms.

2.4   Types of ferrites with respect to their hardness

Ferrites are classified into two categories based on their coercive field strength. They are:

    (i)   Soft ferrite with coercive field strength < 10 Oe

    (ii)   Hard ferrite with coercive field strength > 125Oe

2.4.1 Soft Ferrites

Soft ferrites are those that can be easily magnetized or demagnetized. These are characterized by low coercive forces and high magnetic permeabilities. The low coercivity means the materials magnetization can easily reverse direction without dissipating much energy (hysteresis losses), while the materials high resistivity prevents eddy currents in the core, another source of energy loss, generally exhibit small hysteresis losses. At high frequency metallic soft magnetic materials simply cannot be used due to the eddy current losses. Therefore soft ferrite, which is ceramic insulators, becomes the most desirable material. These materials are ferromagnetic with a cubic crystal structure and the general composition $MO.Fe_2O_3$ where M is a transition metal such as nickel, manganese, magnesium, zinc, cobalt or cadmium. The magnetically soft ferrites first came into commercial production in 1948. Additionally, parts of the family of soft ferrites are the microwave ferrites e.g.Ytrium iron garnet .These ferrite are

used in the frequency range from 100 MHz to 500GHz. For waveguides, for electromagnetic radiation, and in microwave device such as phase shifters. Application of soft ferrite include: cores for electro-magnets, electric motors, transformers, generators, and other electrical equipment. Because of their comparatively low losses at high frequencies they are extremely used in the cores of RF transformers and inductors in the applications such as a switched mode power supplies.

2.4.2 Hard Ferrites

Hard ferrites are difficult to magnetized or demagnetized. Hard magnets are characterized by high remanent inductions and high coercivities. The higher coercivity means the materials are very resistant to becoming demagnetized an essential characteristic for a permanent magnet. They also conduct magnetic flux will and have a high magnetic permeability. This enables these so-called ceramic magnets to store stronger magnetic fields than iron itself. They are cheap and are widely used in household products such as refrigerator magnets. They generally exhibit large hysteresis losses. Hard ferrite referred to as permanent magnets retain their magnetism after being magnetized. Hard ferrite likes Ba-ferrite, Sr-ferrite, Pb-ferrite are used in communication device operating with high frequency currents because of their high resistivity, negligible eddy currents and lower loss of energy due to Joule heating and hysteresis. These are found useful in many applications including fractional horse-power motors, automobiles, audio- and video-recorders, earphones, computer peripherals, and clocks.

2.5 Magnetism and its origin

The word magnetism is used for those physical phenomena, which involve magnetic field and their effect upon materials. The name magnet was used by the Greeks for a stone, which was capable of attracting pieces of the same materials and iron as well. The original magnet (loadstone) is the naturally occurring magnetic iron oxide, i.e. magnetite. Some of magnetite's properties were known to humankind even before 600 B.C.
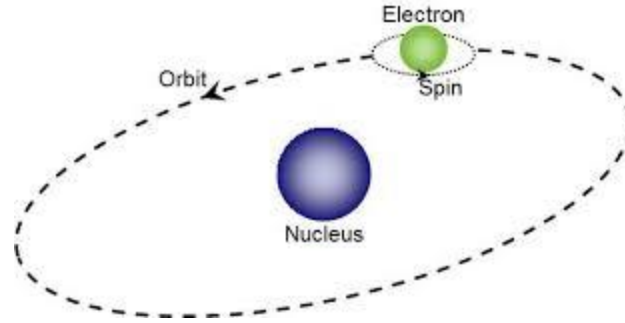
Figure 2.3: Origin of magnetism

Magnetism originates from the spin and orbital magnetic moment of an electron. Magnetism arises from two types of motions of electrons in atoms—one is the motion of the electrons in an orbit around the nucleus, similar to the motion of the planets in our solar system around the sun, and the other is the spin of the electrons around its axis, analogous to the rotation of Earth about its own axis. The orbital and the spin motion independently impart a magnetic moment on each electron causing each of them to behave as a tiny magnet.

2.6   Theory of Initial Permeability

Initial permeability describes the relative permeability of a material at low values of B. The maximum value for μ in a material is frequently a facing of between 2 and 5 or more above its initial value. Low flux has the advantage that every ferrite can be measured at that density without risk of saturation. This consistency means that comparison between different ferrite is easy. For high frequency application, the desirable property of a ferrite is the high initial permeability with low loss. The present goal of the most of the recent ferrite researches is to fulfill this requirement. The initial permeability μ_i is defined as the derivative of induction B with respect to the initial field H in the demagnetization state.

$$\mu_i = \frac{dB}{dH}/H \rightarrow 0, B \rightarrow 0 \tag{2.1}$$

At microwave frequency and also in low anisotropic materials, dH and dB may be in different directions. The permeability is thus a tensor character. In the case of amorphous materials containing a large number of randomly oriented magnetic atoms the permeability will be scalar. As we have

$$B = \mu_0 (H+M) \tag{2.2}$$

and susceptibility

$$\chi = \frac{dM}{dH} = \frac{d}{dxH}\left(\frac{B}{\mu_0} - 1\right) = \frac{1}{\mu_0}(\mu - 1) \tag{2.3}$$

The magnetic energy density

$$E = \frac{1}{\mu_0}\int H.\,dB \tag{2.4}$$

For time harmonic fields $H = H_0$ Sin wt. The dissipation can be described by a phase difference between B^+ and B.

Permeability is namely defines as the proportional constant between the magnetic field induction B and applied intensity H:

$$B = \mu H \tag{2.5}$$

If a magnetic material is subjected to an AC magnetic field as given below:

$$H = H_0 e^{i\omega t} \tag{2.6}$$

Then it is observed that the magnetic flux density B experiences a delay. The delay is caused due to presence of various losses and is thus expressed as

$$B = B_0 \, e^{i\,(\omega t - \delta)} \tag{2.7}$$

Where δ is the phase angle and marks the delay of B with respect to H. The permeability is then given by

$$\mu = \frac{B}{H} = \frac{B_0 e^{i(\omega t - \delta)}}{H_0 e^{i\omega t}}$$

$$= \frac{B_0 e^{-i\delta}}{H_0} = \frac{B_0}{H_0} Cos\delta - i\,\frac{B_0}{H_0}\sin\delta \tag{2.8}$$

$$\mu = \mu' - i\mu'' \tag{2.9}$$

Where $\quad \mu' = \frac{B_0}{H_0}\cos\delta \tag{2.10}$

$$\mu'' = \frac{B_0}{H_0}\sin\delta \tag{2.11}$$

The real Part μ' of complex permeability μ represent the component of B induction which is in phase with H, so it corresponds to the normal permeability. If there is no losses, we should have $\mu = \mu'$, The imaginary part μ'' corresponds to that part of B which is delayed by phase angle δ from H arranging up to 90° from H . The presence of such a component requires a supply of

energy to maintain the alternating magnetization regardless of the origin of delay. The ratio of μ"
to μ' as is evident from equation gives:

$$\frac{\mu'}{\mu''} = \frac{\dfrac{B_0}{H_0}\sin\delta}{\dfrac{B_0}{H_0}\cos\delta} = \tan\delta \qquad (2.12)$$

This tan δ is called the loss Factor or loss tangent. The Q-Factor or quality factor is defined as the reciprocal of this loss factor, i.e.

$$Q = \frac{1}{\tan\delta} \qquad (2.13)$$

And the relative quality factor $= \dfrac{\mu'}{\tan\delta} = \mu' Q$ $\qquad (2.14)$

The behavior of μ' and μ" versus frequency is called the permeability spectrum. The initial permeability of a ferromagnetic or ferrimagnetic substance is the combined effects of the wall permeability and rotational permeability mechanisms. The measurement of complex permeability gives us valuable information about the nature of domain wall and their movements. In dynamic measurements the eddy current loss is very important. This occurs due to the irreversible domain wall movements. The permeability of a ferromagnetic substance is the combined effect of the wall permeability and rotational permeability mechanisms.

2.7 Magnetization Process

Magnetization processes are essentially similar in ferromagnetic metals and ferromagnetic ceramics. The division of a magnetic material into domains explains why, when no field is applied, the magnetic flux is entirely contained within the sample and there is no external manifestation of it. The application of an external field, however, can result in a dynamic increase of magnetization in the sample; an extreme case appears foe a Ni-Fe alloy. A review of the magnetization process, namely the response of ferro-(ferri) magnetic material (bulk) to an applied field with a semi-microscopic approach is presented. In ferro-or ferri-magnetic material, the magnetization curves, especially in low magnetic fields differ widely from sample to sample and as a function of the magnetic history of the sample i.e., of the previous fields which have been successively applied.

2.7.1 Magnetization Curve

For unmagnetized bulk materials, there is a zero net magnetic moment. It can be predicted that there will be an infinite number of degree of magnetization between the unmagnetized and saturation conditions, when the material is subjected to an external magnetic field. The increase in magnetic field leads to domain wall displacements unit all the domains with orientations opposite to the field have been substituted by domain with direction parallel to H. However, there might be domains with orientation neither opposite nor parallel; also the applied field can have an orientation which does not coincide with an easy direction. These extreme situations are corresponds respectively to random orientation of domains complete alignment is one direction with elimination of domain walls. If we start with a demagnetized specimen and increase the applied magnetic field, the bulk material will progressively magnetized by the domain dynamics. The magnetization of the sample will follow the course as shown in Figure 2.4 [Smit and Wijn, 1959]. The slop from the origin to a point on the curve r the ratio $\frac{M}{H}$ is defined as magnetic susceptibility. This curve is called magnetization curve. This curve is generally perceived as being made of three major portions.

This magnetization mechanism takes place at high fields; it involves higher energies because the field has to overcome the anisotropy field to produce spin reversal. In contrast, domain wall motion occurs by the progressive reversal of a small fraction of spins, from an easy direction to another one. Magnetization processes can be affected by stress [Goldman, 1999; Valenzuela, 1994; Spaldin, 2003]. This phenomenon known as stress anisotropy is related to magnetostriction can also be explained on the basis of the spin-orbit coupling.
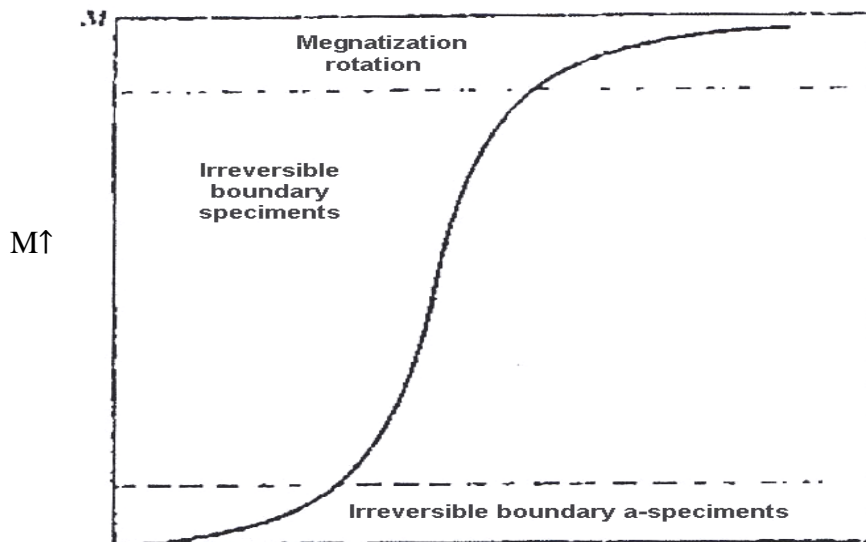
$$\rightarrow H$$

$$\rightarrow \mathrm{H}$$

Figure 2.4: Domain dynamics during various parts of the magnetization curve

The first, the lower section, is the initial susceptibility region and characterized by reversible domain wall movements and rotations. By reversible means that after the magnetization slightly with an increase in field the origin magnetization can be reversed if the field is reduced to initial value. The condition of the displacement walls to an initial permeability is entirely dependent on the sort of material studied. In the second stage magnetization curve if the field is increased, the intensity of the magnetization increases more drastically is called the irreversible magnetization range. This range is obtained mainly by the reversible domain wall motion from one stable state to another.

If the field is increased further, the magnetization curve less step and its process become reversible once more. In the third section of magnetization curve, the displacement of domain walls have all ready been completed and the magnetizations take place by rotation magnetization. This range is called rotation magnetization range. Beyond this range the magnetization gradually approaches to saturation magnetization shown in Figure 2.4.

2.8　Dielectric Constant

Dielectric material slight shift of the charges from their average equilibrium positions is a cause of dielectric polarization, which creates an internal electric field and opposite to the direction of external field. Dielectric is the electrically insulating material between the metallic plates of a capacitor, as well as the polarization of the dielectric by the applied electric field increases the capacitor's surface charge. Dielectric constant is defined as the ratio of the capacitance of a capacitor filled with a given dielectric to the capacitance of the same capacitor with vacuum. It is a number without dimensions, a quantity measuring the ability of a substance to store electrical energy in an electrical field. If C represents the capacitance of a capacitor with dielectric and C_0 represents the capacitance of the same capacitor with vacuum, then the dielectric constant (ε') can be given by,

$$\varepsilon' = \frac{C}{C_o} \tag{2.15}$$
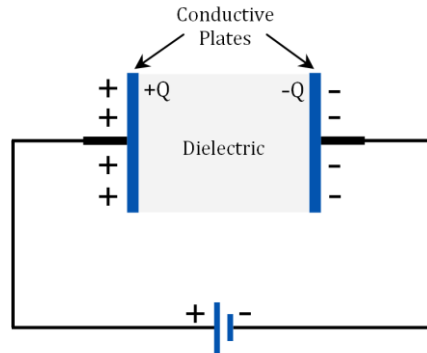
Figure 2.5: Schematic illustration of capacitive cell

But capacitance C of a parallel plate capacitor can be expressed as

$$C = \frac{\varepsilon A}{d} \tag{2.16}$$

where, A is the area of each plate, d represents the separation between the plates and ε represents the permittivity of the dielectric material within the cpacitor.

If ε_o represents the permittivity of the free space, then from equation (2.15) we get

$$\varepsilon' = \frac{\varepsilon}{\varepsilon_o} \tag{2.17}$$

Therefore, dielectric constant can also be defined as the ratio of the permittivity of a substance to the permittivity of free space. It is an expression of the extent to which a material concentrates electric flux, and is the electrical equivalent of relative magnetic permeability.

2.8.1 Dependence of Dielectric Constant on Frequency

Polarization under the effect of direct current leads to a fixed value dielectric current. The orientation polarization is continuously changes due to continuous change in the orientation of molecules with the ac field, the molecules orientation changing from one way to the other way. The energy dissipated in a dielectric is called dielectric loss. The dielectric loss in the radio frequency region is usually due to dipole rotation or the ions jumping from one equilibrium position to another. Polarization systems respond to an electrical field by shifting their masses around and forms dipoles. These shifted masses are accelerated and de-accelerated with the change of the applied field which takes some time. Therefore, the polarization mechanism of a

system depends on the frequency of the applied electrical field. Alternating electrical field induces alternating forces to the dipoles. Since the dipole response to a field involves the movement of masses, inertia will prevent the arbitrarily fast movements. When the frequency of the applied field increases, this movement of dipoles also increases. At high frequency, the dipoles are unable to cope with it. So at very high frequencies all movement of dipoles will 'die out' and there will be no response of the dipoles to the frequency field [Dai *et al.,* 2012]. Dielectric constant (ε') is a measure of polarization of a system, it also depends on the frequency of the applied field. In general as frequency increases, its dielectric constant drops. But for some material the dielectric constant can increase with the increase in frequency due to the parasitic effect but only at the low temperature. Due to the finite conductivity of dielectric materials are significant energy loss occurs in the form of heat. Molecules with permanent dipole moment are not desirable as they have high dielectric losses at high frequency.

2.9   DC Resistivity of Ferrites

Extensive investigation into the origin of the electrical conductivity of the spinels has been carried out by [Verwey *et al.,* 1947; and Jonker, 1959]. The resistivity of ferrites at room temperature can vary, depending on chemical composition between about 10^{-2} to higher than 10^{+11} ohm-cm. The low value of resistivity is due to the simultaneous presence of ferrous and ferric ions on equivalent lattice sites (octahedral). For example Fe_3O_4 at room temperature has resistivity of approximately 7×10^{-3} Ohm-cm and Fe_2O_4 with some deficiency in iron and sintered in a sufficiently oxidizing atmosphere so that the product contains no ferrous ions can have a resistivity higher than 7×10^6 ohm-cm. To make high resistivity ferrites one must sure that there are no ferrous ions in the stoichiometric ferrites.

Temperature dependent resistivity of ferrites follows Arrhenius relation [Smit and Wijn, 1959]:

$$\rho = \rho_0 e^{\frac{E_a}{kT}} \qquad (2.18)$$

Where ρ is the resistively and E_a is the activation energy required for hopping of an electron from one lattice site to another.

2.10   Microstructure

A polycrystal is much more than many tiny crystals bonded together. The interfaces between the crystals, or the grain boundaries which separate and bond the grains, are complex

and interactive interfaces. The whole set of a given material's properties of mechanical, chemical and especially electrical and magnetic depend strongly on the nature of the microstructure. The grain boundary is the region, which accommodates the difference in crystallographic orientation between the neighboring grains. For certain simple arrangements, the grain boundary is made of an array of dislocations whose number and spacing depends on the angular deviation between the grains. The ionic nature of ferrites leads to dislocation patterns considerably more complex than in metals, since electrostatic energy accounts for a significant fraction of the total boundary energy. For low-loss ferrite, Goldman 1999 states that the grain boundaries influence properties by [Yan and Johnson, 1978]

  (i)   creating a high resistivity intergranular layer,

 (ii)   acting as a sink for impurities which may act as a sintering aid and grain growth modifiers,

(iii)   Providing a path for oxygen diffusion, which may modify the oxidation state of cations near the boundaries.

    In addition to grain boundaries, ceramic imperfections can impede domain wall motion and thus reduce the magnetic property. Among these are pores, cracks, inclusions, second phases, as well as residual strains. Imperfections also act as energy wells that pin the domain walls and require higher activation energy to detach. They affect the domain dynamics and are responsible for a much greater share of the degradation of properties than would expect grain growth kinetics depends strongly on the impurity content. A minor do pant can drastically change the nature and concentration of defects in the matrix, affecting grain boundary motion, pore mobility and pore removal [Yan and Johnson, 1978]. The effect of a given do pant depends on its valence and solubility with respect to host material. If it is not soluble at the sintering temperature, the do pant becomes a second phase which usually segregates to the grain boundary.
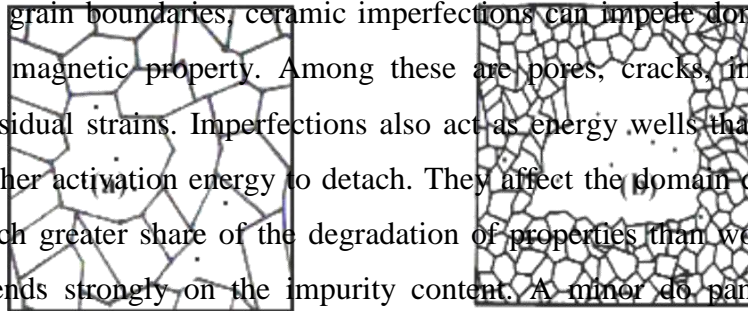
Figure 2.6: Grain growth (a) discontiuous, (b) duplex (schematic) [Goldman, 1999]

The porosity of ceramic samples results from two sources, intragranular porosity and intergranular porosity, Figure 2.6. An undesirable effect in ceramic samples is the formation of exaggerated or discontinuous grain growth which is characterized by the excessive growth of some grains at the expense of small, neighboring ones, Figure 2.7. When this occurs, the large grain has a high defect concentration. Discontinuous growth is believed to result from one or several of the following: powder mixtures with impurities; a very large distribution of initial particle size; sintering at excessively high temperatures; in ferrites containing Zn and /or Mn, a low O^2 partial pressure in the sintering atmosphere. When a very large grain is surrounded by smaller ones, it is called 'duplex' microstructure. Grain boundaries begin to form at the interface between at least three contacting particles. Pores appear as voids between at least three contacting particles. Grain growth begins during the intermediate stage of sintering. Since grain boundaries are the sinks for vacancies, grain growth tends to decrease the pore elimination rate due to the increase in distance between pores and grain boundaries and by decreasing the total grain boundary surface area.

(a)   (b)
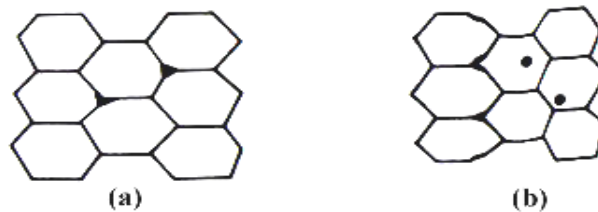
Figure 2.7: Porosity character: (a) intergranular (b) intragranular [Valenzula, 1994]

Grain growth kinetics depends strongly on the impurity content. A minor dopant can drastically change the nature and concentration of defects in the matrix, affecting grain boundary motion, pore mobility and pore removal [Valenzula, 1994; Cullity, 1972]. The effect of a given dopant depends on its valence and solubility with respect to host material. If it is not soluble at the sintering temperature, the dopant becomes a second phase, which usually segregates to the grain boundary.

CHAPTER III

EXPERIMENTAL PROCEDURE

EXPERIMENTAL PROCEDURE

3.1   Methodology of Rare Earth Ferrite Preparation

The preparation of rare earth ferrites with optimum desired properties is still a complicated and elaborate task. In this chapter, experimental methods of sample preparation techniques of rare earth Yttrium doped Ni-Zn ferrites are described briefly. We have described also the effect of the preparation, calcinations and sintering process of the rare earth substituted Ni-Zn ferrites with the general formula $Ni_{0.25}Zn_{0.75}Y_xFe_{2-x}O_4$. The rare earth ferrite is not completely defined by its chemistry and crystal structure but also requires knowledge and control of parameters of its microstructure such as density grain size, porosity and their intra and intergranular distribution. Rare earth ions can improve densification and increase permeability and resistivity. In $Ni_{0.25}Zn_{0.75}Y_xFe_{2-x}O_4$ ferrites where Yttrium enters into the B-sites by displacing a proportionate number of Fe^{3+} form 'B' to 'A' sites.

It is well known that almost all rare-earth ferrites decompose at the elevated temperature if we want to melt them under normal conditions. This happens because the oxygen splits off at higher temperature reducing Fe^{3+} and Fe^{+2}. This necessarily implies that ferrite preparation by melting, as in case of metals, is impossible. The normal methods of preparation of ferrites comprise of the conventional ceramic method or powder metallurgy, chemical co-precipitation method, sol-gel method, wet method etc. In this work Conventional Ceramic Method has been employed for the preparation of $Ni_{0.25}Zn_{0.75}RE_x$ ferrites for its relative similarity and availability.

3.2   Composition of the Studied Ferrites

In the present work the various compositions of rare earth (Y) substituted Ni-Zn ferrites are synthesized, characterized and investigated. The ferrite sample preparation facility is available in Solid State physics Lab at Khulna University of Engineering and Technology (KUET). The ferrites under investigation are:

(i) $Ni_{0.25}Zn_{0.75}Fe_2O_4$

(ii) $Ni_{0.25}Zn_{0.75}Y_{0.02}Fe_{1.98}O_4$

(iii) $Ni_{0.25}Zn_{0.75}Y_{0.04}Fe_{1.96}O_4$

(iv) $Ni_{0.25}Zn_{0.75}Y_{0.06}Fe_{1.94}O_4$

(v) $Ni_{0.25}Zn_{0.75}Y_{0.08}Fe_{1.92}O_4$
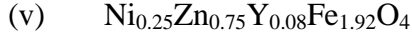
3.3   Sample Preparation Technique

Structural and magnetic properties of rare earth substituted Ni-Zn ferrites are greatly dependent on fabrication technique. A goal common to all the ferrites is the common formation of the spinel structure. The large majority of ferrite powders are made by the conventional Ceramic process or Solid State Reaction method. Most non-conventional process involves producing the powder by a wet method. Among these methods, some are [Goldman, 1999] Co-precipitation, Organic precursors, Sol-gel synthesis, Spray-drying, Freeze-drying, Glass crystallization etc.

In the present research, we prepared our sample $Ni_{0.25}Zn_{0.75}Y_xFe_{2-x}O_4$ [Where x = 0.00, 0.02, 0.04, 0.06 and 0.08] by Solid state reaction technique.

3.3.1 Solid State Reaction Method

In the solid state reaction method, the required composition is usually prepare from the appropriate amount of raw mineral oxides or carbonates by crushing, grinding and milling [Kittel, 1996]. Solid state reaction occurs between apparently regular crystal lattices, in which the kinetic motion is very much restricted and it depends on the presence of lattice defects [Nelson and Riely, 1945]. In solid state reaction method, appropriate amounts of two or more component of chemical compounds are carefully grinded together and mixed thoroughly in mortar with pestle or ball milling with appropriate homogenization. Solid oxides do not usually react together at room temperature over normal time scale and it is necessary to heat them at much higher temperatures. The ground powders are then calcined in air or oxygen at a temperature 850°C. Sometime this process is continued until the mixture is converted into the correct crystalline phase. The calcined powders are then further crushed into fine powders. The pellets or disc shaped and toroid shaped samples are made of these calcined powders using uniaxial or iso-static pressure. Sintering is carried out in the solid state, at temperatures 1150°C, for times of typically 1- 5 hours in air.

The overall preparation process generally comprised of the following four major steps are:

(i)   Preparing a mixture of desired composition

(ii)   Pre sintering the mixture to form ferrite

30

(iii)   Converting the Raw ferrite into powder and pressing the powder

(iv)   Sintering.

3.3.2 Flow Chart of Sample Preparation

The following block diagram in Figure 3.1 represents the method employed for the rare -earth ferrites:
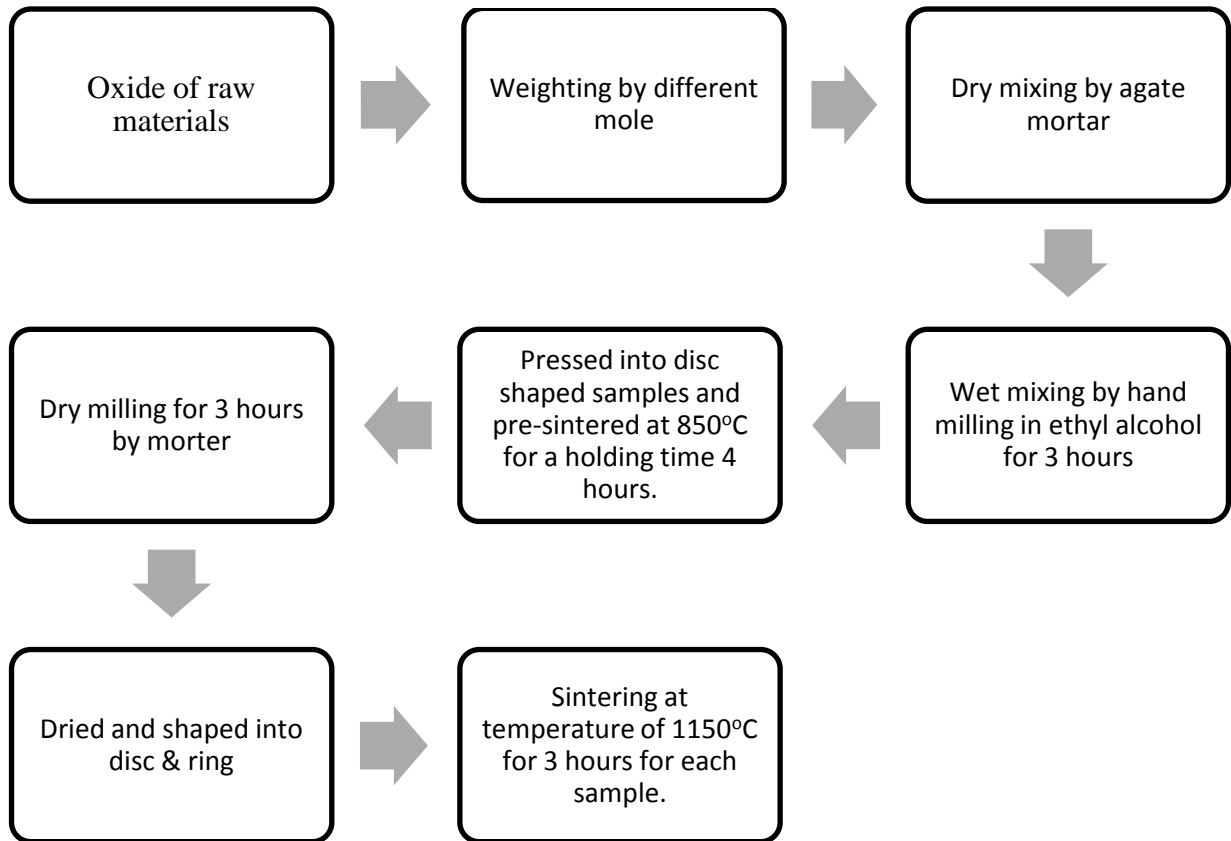
Figure 3.1:   Flow chart of rare-earth ferrite sample preparation technique by usual ceramic method.

3.4   Sample preparation

High purity powders of NiO (99.9%), ZnO (99.9%), Y_2O_3 (99.9%), Fe_2O_3 (99.9%) were used as the raw materials. The exact amounts of compounds were calculated for each composition. Using those raw materials were weighed and mixed thoroughly by hand milling. During hand milling, few drops of acetone were added to increase the degree of mixing. The

mixture was pre-sintered at 850ºC for 4 hours. The calcined powder again was crashed into fine powders. From the fine powders , toroid and disk -shaped samples were prepared and sintered at 1150° C for 3 hours. After sintering the sample we got the final product and we studied the electrical and magnetic properties of the desired sample.

3.4.1 Calculation for sample preparation

For the polycrystalline $Ni_{0.25}Zn_{0.75}Y_xFe_{2-x}O_4$ [Where x=0.00, 0.02, 0.04, 0.06 and 0.08] arrangement we used NiO, ZnO, Y_2O_3 and Fe_2O_3. The weight percentage of the oxide to be mixed for various samples was calculated by using formula:

$$\text{Weight \% of oxide} = \frac{M.wt \cdot of\ oxide \times required\ weight\ of\ the\ sample}{Sum\ of\ Mol.wt.of\ each\ oxide\ in\ a\ sample}$$

To get exact amount of each of the compounds the detail calculations are shown in following three tables.

Table 3.1: Atomic /molecular mass of raw materials

.

Name of compound/atom	Molecular / Atomic mass(g/mol)
NiO	74.69
ZnO	81.39
Y_2O_3	225.82
Fe_2O_3	159.70
Ni	58.69
Zn	65.39
Y	88.91
Fe	55.85
O	16

Table 3.2: Calculation of total mass of the composition.

Composition	Mass of the sample (g)
$Ni_{0.25}Zn_{0.75}Fe_2O_4$	$(58.69\times.25)+(65.39\times.75)+(55.85\times2)+(16\times4)=239.415$
$Ni_{0.25}Zn_{0.75}Y_{0.02}Fe_{1.98}O_4$	$(58.69\times.25)+(65.39\times.75)+(88.91\times.02)+(55.85\times1.98)+(16\times4)=240.076$
$Ni_{0.25}Zn_{0.75}Y_{0.04}F_{1.96}O_4$	$(58.69\times.25)+(65.39\times.75)+(88.91\times.04)+(55.85\times1.96)+(16\times4)=240.737$
$Ni_{0.25}Zn_{0.75}Y_{0.06}Fe_{1.94}O_4$	$(58.69\times.25)+(65.39\times.75)+(88.91\times.06)+(55.85\times1.94)+(16\times4)=241.399$
$Ni_{0.25}Zn_{0.75}Y_{0.08}Fe_{1.92}O_4$	$(58.69\times.25)+(65.39\times.75)+(88.91\times.08)+(55.85\times1.92)+(16\times4)=242.06$

Table 3.3:   Calculation for 20 g sample preparation

Composition	Need of NiO(g)	Need of ZnO(g)	Need of Fe_2O_3(g)	Need of Y_2O_3(g)
$Ni_{0.25}Zn_{0.75}Fe_2O_4$	$(74.69\times0.25\times20)/239.415=1.5599$	$(81.39\times0.75\times20)/239.415=5.0993$	$(159.70\times20)/239.415=13.3409$	N/A
$Ni_{0.25}Zn_{0.75}Y_{0.02}Fe_{1.98}O_4$	$(74.69\times0.25\times20)/240.076=1.5556$	$(81.39\times0.75\times20)/240.076=5.0852$	$(159.70\times1.98\times20)/(2\times240.076)=13.1712$	$(225.82\times0.02\times20)/(2\times240.076)=0.1881$
$Ni_{0.25}Zn_{0.75}Y_{0.04}Fe_{1.96}O_4$	$(74.69\times0.25\times20)/240.737=1.5513$	$(81.39\times0.75\times20)/240.737=5.0712$	$(159.70\times1.96\times20)/(2\times240.737)=13.0712$	$(225.82\times0.04\times20)/(2\times240.737)=0.3752$
$Ni_{0.25}Zn_{0.75}Y_{0.06}Fe_{1.94}O_4$	$(74.69\times0.25\times20)/241.399=1.5471$	$(81.39\times0.75\times20)/241.399=5.0573$	$(159.70\times1.94\times20)/(2\times241.399)=12.8342$	$(225.82\times0.06\times20)/(2\times241.399)=0.5613$
$Ni_{0.25}Zn_{0.75}Y_{0.08}Fe_{1.92}O_4$	$(74.69\times0.25\times20)/242.06=1.5428$	$(81.39\times0.75\times20)/242.06=5.0435$	$(159.70\times1.92\times20)/(2\times242.06)=12.6673$	$(225.82\times0.08\times20)/(2\times242.06)=0.7463$

3.4.2 Mixed and Milled the Samples (Hand Milling)

Samples were weighed according to the calculation and then mixed thoroughly by solid state reaction method. Each of the compositions was grinded for four hours using agate mortar and pestle. The following figure shows the hand milling set up.

Figure 3.2:   Raw materials in agate mortar with pestle.

3.4.3 Pre-sintering the Mixture to form Ferrite
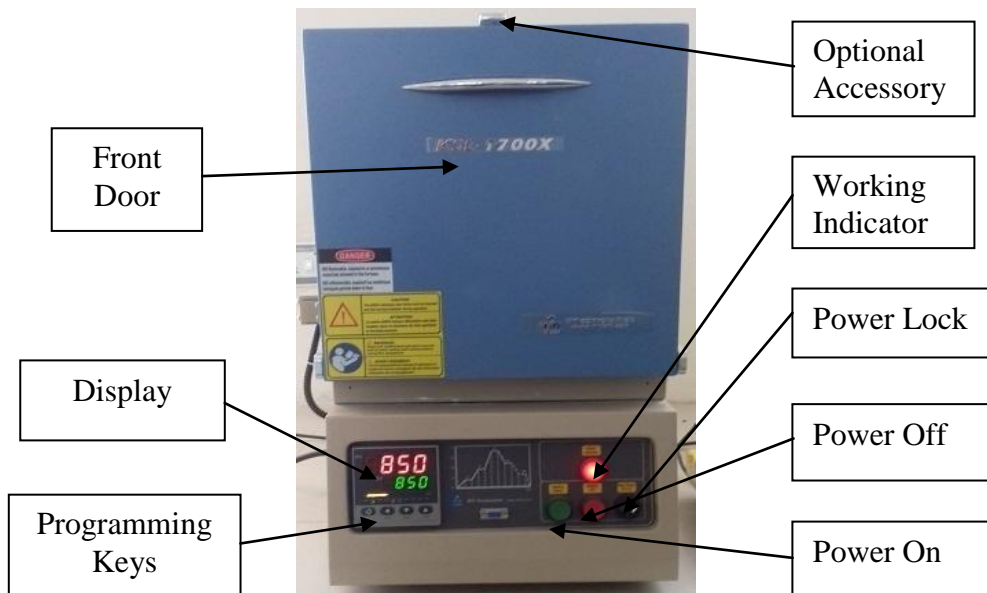
Figure 3.3: Furnace (*KSL-1700X* made in USA) in the solid state physics laboratory, KUET.

Pre-sintering is a process of obtaining a homogeneous and pure sample of mixed powders by heating them for a certain time at a high temperature below the sintering temperature. It is

done to increase the strength green compact and remove the lubricants and binders added during blending. During the Pre-sintering stage, the reaction of Fe_2O_3 with metal oxide/carbonate (say, MeO or $MeCO_3$) takes place in the solid state to form spinel according to the reactions:

$$MeO + Fe_2O_3 \longrightarrow MeFe_2O_4 \text{ (Spinel)}$$

$$Fe_2O_3 + MeCO_3 \longrightarrow MeFe_2O_4 + CO_2$$
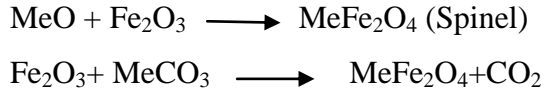
3.4.4 Pressing or Extrusion

Powder pressing is the compaction of powders into a geometric form. Pressing is usually performed at room temperature. This creates a solid part called a green compact. The strength of this pressed, unsintered part, (green strength), is dependent on compactability, binders may be used to increase compactibility.

Figure 3.4: Hydraulic press and dies for preparing sample

Table 3.4: Various Shape and size of $Ni_{0.25}Zn_{0.75}Y_xFe_{2-x}O_4$ sample

Shape	Weight (gm)	Name of the sample:$Ni_{0.25}Zn_{0.75}Y_xFe_{2-x}O_4$ [Where x=0.00, 0.02, 0.04, 0.06 and 0.08]					Purpose
		X=0.00	X=0.02	X=0.04	X=0.06	X=0.08	
Ring	1 gm						Permeability
Pellet	.6 gm						VSM, XRD
Pellet	.4 gm						Dielectric, Resistivity
Pellet	.2 gm						SEM

3.4.5 Sintering

Sintering is a process of compacting and forming a solid by heat treatment. In this process the atoms in the materials diffuse across the boundaries of the particles, fusing the particles together and creating one solid piece. Sintering process takes places without melting the sample i.e. heating the sample below its melting point. Sintering is the final step in which sintering temperature, sintering time as well as the atmosphere of the furnace play very important role on the magnetic property of final samples.

KSL-1700X-S Furnace

KSL-1700X-S is a compact design high temperature muffle furnace designed for maximum energy saving ($<1KW$ at $10°$ C/min).It is an ideal tool for materials annealing and sintering in research laboratory.

  ➢ The furnace consists of high quality alumina fiber brick and MoSi2 heating elements with double layer case.
  ➢ Gas inlet and venting port are installed for using at oxygen or inert gas riched atmosphere.
  ➢ Design of sliding down door is for loading sample at easy.

➢ The furnace temperature is controlled by high precision SCR(Silicon Controlled Rectifier) digital controller with accuracy +/-1°C and 30 segments programmable up to 1700°C.

Figure 3.5: High Temperature Muffle Furnace (KSL-1700X-S) at Solid State Physics Lab, KUET.

Illustration of Temperature Segment Setting for Sintering
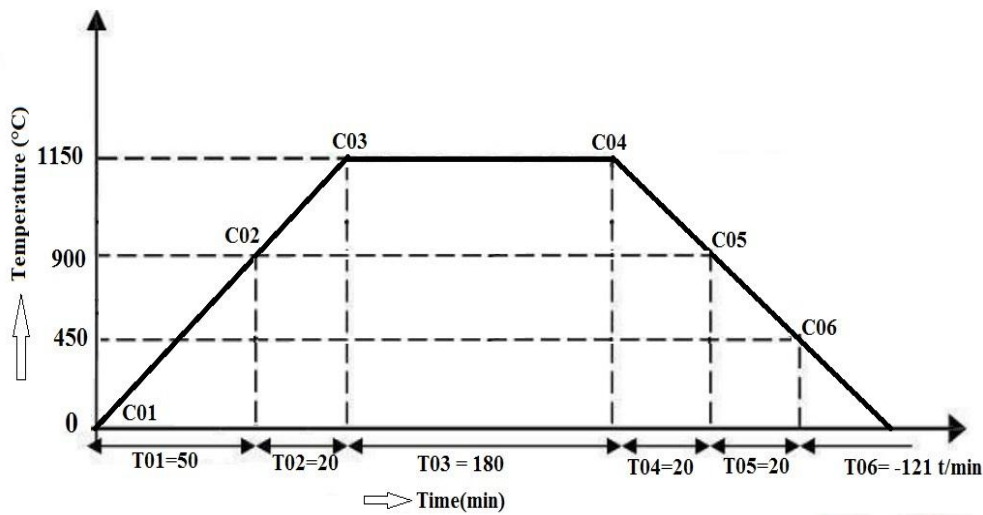
Figure 3.6: Graphical presentation of temperature control program segments.

37

3.5 Sample Preparation at a glance

Oxide of raw materials

Weighing by different Mole percentage

Hand milling for 4 hours

Pre-sintering at 850^0C for 2 hours

Grinding for 2 hours

Sample placed into different dies

Pressing to desired shapes

Sintering at 1150^0C for 3 hours

Final Product
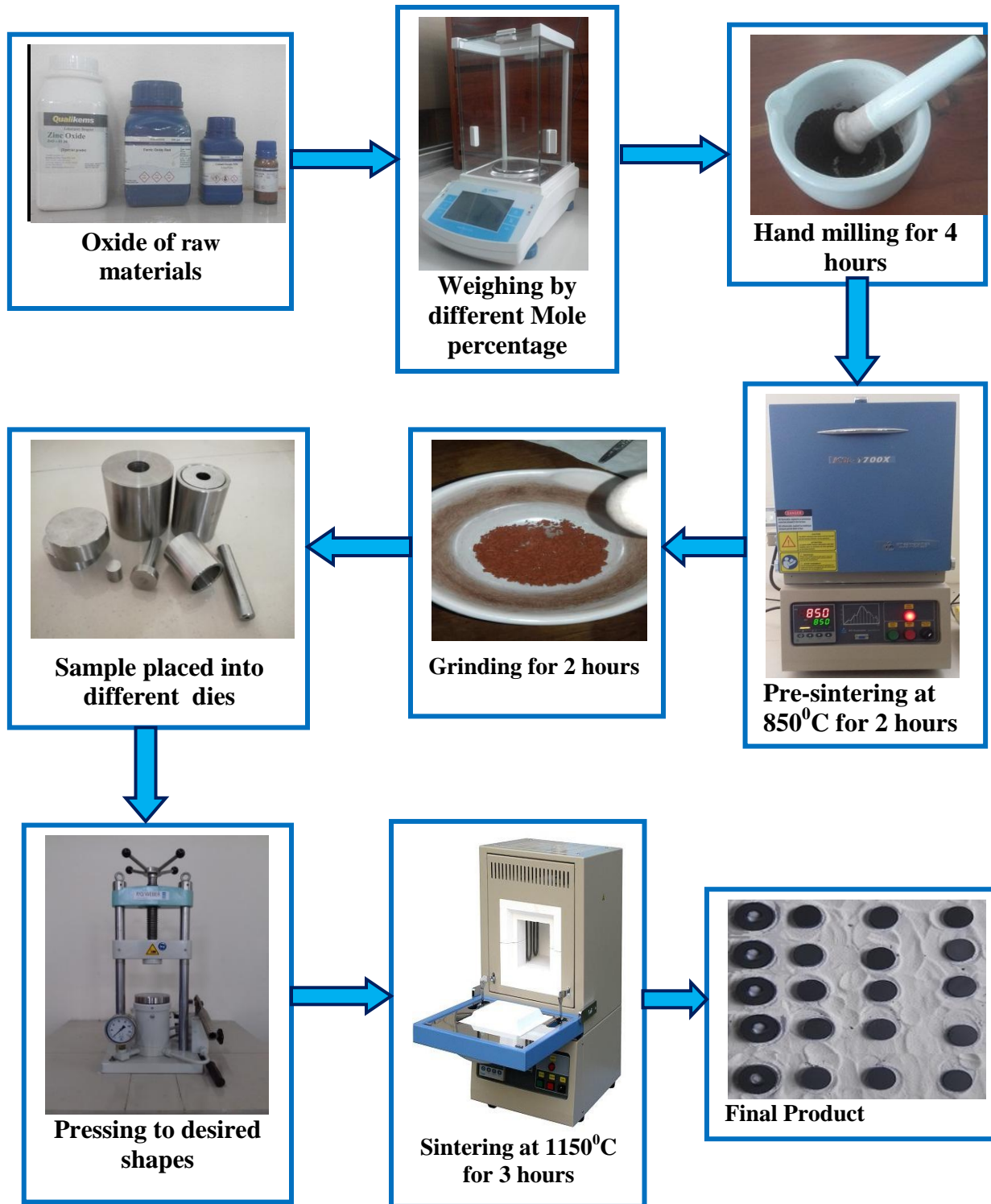
The $Ni_{0.25}Zn_{0.75}Y_xFe_{2-x}O_4$ sample was sintered at $1150°$ C. High Temperature Muffle Furnace (KSL-1700X-S) at Solid State Physics Lab, KUET was used for sintering the sample. According

to the Furnace operational manual the temperature Control Program was taken with 6-segments as shown in Figure 3.6.

Table 3.5: Temperature Control Program with 6-segments

Prompt	Input Data	Description
C01	0	Initial Temperature
T01	50	Furnace took 50 min from 0-900° C in the 1st segment
C02	900	Target temperature of the 1st heat-up stage
T02	20	Furnace took 20 min from 900-1150° C in the 2nd segment
C03	1150	Target temperature of the 3rd heat-up stage
T03	180	Furnace kept 180 minutes at $1150^{o}C$ in the 3rd segment
C04	1150	Target temperature of the fourth stage
T04	20	Cooling time 20 minutes from $1150\text{-}900^{o}C$
C05	900	Target temperature of the fifth cooling stage
T05	20	Cooling time 20 minutes from $900\text{-}450^{o}C$
C06	450	Temperature of the sixth stage
T06	-121	Program end, Out-put power off. Furnace cooling down naturally. (T06 = -121 is an order to stop running)

3.6   X-ray Diffraction

X-ray diffraction (XRD)is a scattering of X-rays by the atoms of a crystal that produces an interference effect so that the diffraction pattern gives information on the structure of the crystal or the identity of a crystalline substance.XRD is a rapid analytical technique primarily used for phase identification of a crystalline material and can provide information on unit cell dimensions. It provides precise knowledge of the lattice parameter as well as the substantial information on the crystal structure of the material under study.XRD is based on constructive interference of monochromatic X-ray diffraction from a crystalline sample where crystalline substances act as three-dimensional diffraction gratings with grating constant equal to the spacing of planes in the crystal lattice. The interaction of the incident X-rays with the sample produces constructive interference when satisfying the Bragg's condition:

$$2d \sin \theta = n\lambda \qquad\qquad (3.1)$$

This law relates the wavelength of electromagnetic radiation to the diffraction angle and the lattice spacing in a crystalline sample. Typically, this is achieved by comparison of d-spacing's with standard reference patterns.
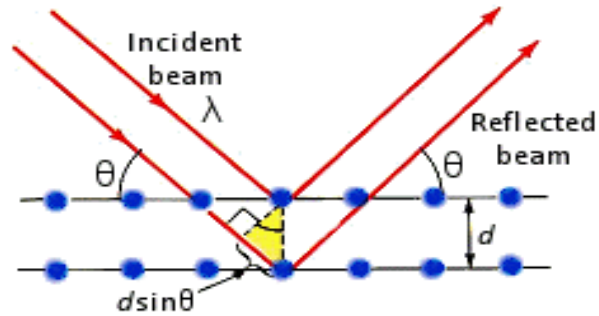
Figure 3.7: Bragg diffraction of x-rays from successive planes of atoms

3.6.1 Different Parts of the PHILIPS X'Pert PRO XRD System
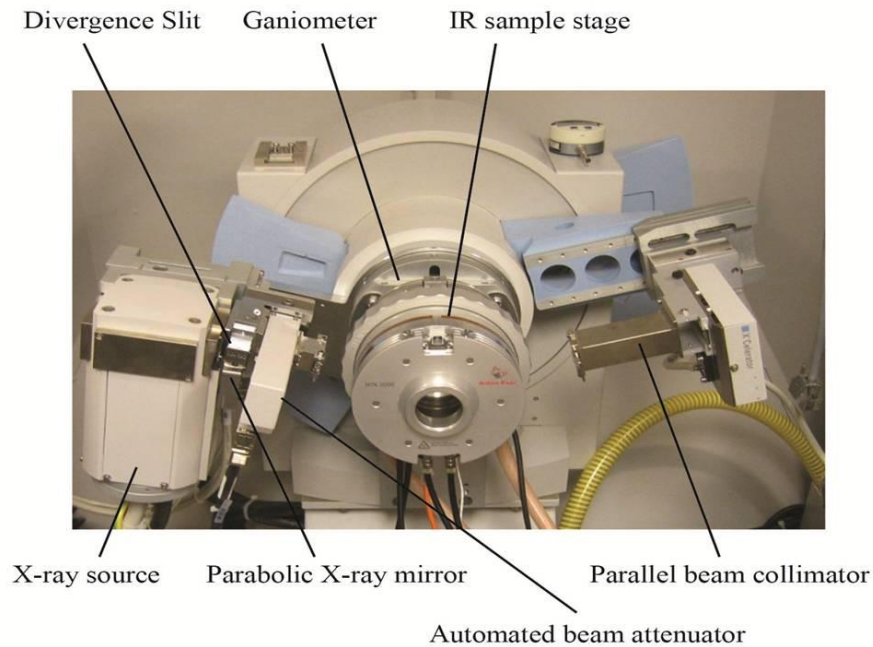
Figure 3.8: Internal arrangement of a PHILIPS X' Pert PRO X-ray diffractometer

In this research, Phillips X'pert PRO X-ray diffractometer of Atomic Energy Centre, Dhaka was used. The wavelength of the used X-ray is ($\lambda = 1.5418$ Å) and is of the same order of magnitude as that of the lattice constant of crystals and this makes it so useful in structural analysis of crystal structure.

3.6.2 Interpretation of the XRD data

The XRD data consisting of θ_{hkl} and d_{hkl} values corresponding to the different crystallographic planes are used to determine the structural information of the samples like lattice parameter and constituent phase. Lattice parameters of Co-ferrites samples were determined. Normally, lattice parameter of an alloy composition is determined by the Debye-Scherrer method after extrapolation of the curve. We determine the lattice spacing (interplanerdistance), d using these reflections from the equation which is known as Bragg's Law.

$$2d_{hkl}Sin\theta = \lambda, \qquad \qquad \text{i.e. } d_{hkl} = \frac{\lambda}{2\sin\theta} \qquad \qquad (3.2)$$

where λ is the wavelength of the X-ray, θ is the diffraction angle and n is an integer representing the order of the diffraction.

3.6.3 Lattice Parameter

The lattice parameter for each peak of each sample was calculated by using the formula:

$$a = d_{hkl} \times \sqrt{h^2 + k^2 + l^2} \qquad \qquad (3.3)$$

Where h, k, l are the indices of the crystal planes. We get d_{hkl} values from the computer using software "X' Pert HJGHS CORE". So we got ten 'a' values for ten reflection planes such as a_1, a_2, a_3 ….. etc. Determine the exact lattice parameter for each sample, through the Nelson-Riley extrapolation method. The values of the lattice parameter obtained from each reflected plane are plotted against Nelson-Riley function [Tahir Abbas *et al.* , 1995]. The Nelson-Riley function F (θ), can be written as

$$F(\theta) = \frac{1}{2}\left[\frac{\cos^2\theta}{\sin\theta} + \frac{\cos^2\theta}{\theta}\right] \qquad \qquad (3.4)$$

Where θ is the Bragg's angle. Now drawing the graph of 'a' vs. $F(\theta)$ and using linear fitting of those points will give us the lattice parameter 'a_0'. This value of 'a_0' at $F(\theta) = 0$ or $\theta = 90°$ .These 'a_0's are calculated with an error estimated to be $\pm 0.0001\text{Å}$.

3.6.4 X-ray Density and Bulk Density

X-ray density, ρ_x was also calculated usual from the lattice constant. The relation between ρ_x and 'a' is as follows,

$$\rho_x = \frac{ZM}{Na^3} \tag{3.5}$$

where M is the molecular weight of the corresponding composition, N is the Avogadro's number $(6.023\text{X}10^{23}$ mole^{-1}), 'a' is the lattice parameter and Z is the number of molecules per unit cell, $(Z = 8$ for the spinel cubic structure). The bulk density was calculated considering a cylindrical pellet of mass (m) and volume (V) of the pellets using the relation

$$\rho_B = \frac{mass\,of\,the\,samples}{volume\,of\,the\,sample} = \frac{m}{V} = \frac{m}{\pi r^2 h} \tag{3.6}$$

Where m is the mass of the pellet sample, r is the radius and h is the thickness of the pellet.

3.6.5 Porosity

Porosity is the amount of spaces in between sediments. Porosity is a parameter which is inevitable during the process of sintering of oxide materials. It is noteworthy that the physical and electromagnetic properties are strongly dependent on the porosity of the studied samples. Therefore an accurate idea of percentage of pores in a prepared sample is prerequisite for better understanding of the various properties of the studied samples to correlate the microstructure property relationship of the samples under study.

Pore Space
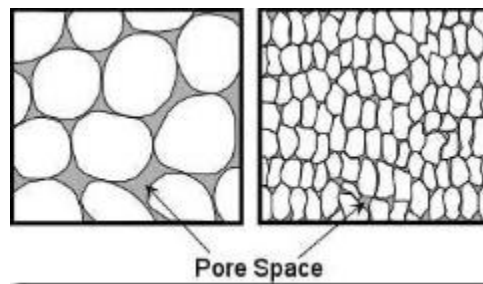
Figure 3.9:   Porosity

The porosity of a material depends on the shape, size of grains and on the degree of their storing and packing. The difference between the bulk density ρ_B and X-ray density ρ_x gave us the

measure of porosity. Percentage of porosity has been calculated using the following relation [Smit and Wijin 1959]].

$$P = \left(1 - \frac{\rho_B}{\rho_x}\right) \times 100\%$$
(3.7)

3.7   Surface morphology and microstructure

The microstructural study was performed in order to have an insight of the grain structures. The samples of different compositions were chosen for this purpose. The samples were visualized under a High-resolution Scanning Electron Microscope (SEM) images. Average grain sizes of the samples were determined from SEM micrographs by linear intercept technique [Hossain, 1998]. To do this, several random horizontal and vertical lines were drawn on the micrographs. Therefore, we counted the number of grains intersected and measured the length of the grains along the line traversed. Finally the average grain size was calculated.

3.7.1 Scanning Electron Microscope

Scanning Electron Microscope (SEM) is a type of electron microscope that creates various images by scanning the surface of the sample. SEM is one kind of surface morphology where a high energy beam of electrons are focused on the surface of a sample and detecting signals from the interaction of the incident electron with the sample's surface.

Figure 3.10:   Scanning Electron Microscope

In SEM process signals come from the primary beam impinging upon the sample and from other interactions within the sample near the surface. The SEM is capable of producing high resolution images of a sample surface in its primary use mode, secondary electron imaging. Characteristic x-rays are emitted when the primary beam causes the ejection of inner shell electrons from the sample and are used to tell the elemental composition of the sample. The back-scattered electrons emitted from the sample may be used alone to form an Image.

3.8 Permeability Measurement

3.8.1 Wayne Kerr Precision Impedance Analyzer

The Wayne Kerr Technologies 6500B series of Precision Impedance analyzer provides impedance measurement capability of components from 20Hz up to 120 MHz. A comprehensive range of functions enables a component to be accurately characterized over a wide frequency range with a choice of Analysis and meter modes allowing swept, single and repetitive measurements. The Graphical User Interface (GUI) combined with the large touch screen TFT display enables measurement parameters to be modified easily and quickly Figure 3.11. The instrument may be remotely controlled using the GPIB or LAN interface.
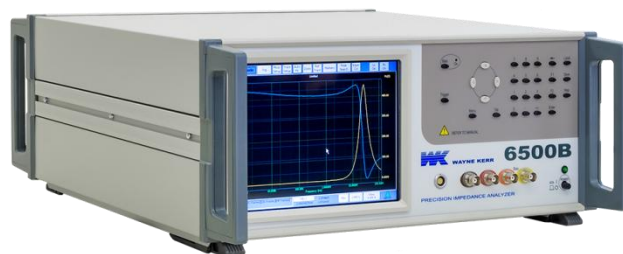
Figure 3.11:   Wayne Kerr Impedance analyzer (6500B series) in solid state physics laboratory, KUET

A comprehensive range of AC functions enables a wide range of components to be measured accurately. Each measurement displays two user selectable components, which allow specific component characteristics to be monitored. Any of the following parameters can be measured and displayed.

Table 3.6

AC Measurement parameters
➢ Impedance (Z)
➢ Inductance (L)
➢ Resistance (R)
➢ Capacitance (C)
➢ Phase Angle (θ)
➢ Dissipation Factor(D)
➢ Quality Factor (Q)
➢ Reactance (X)
➢ Conductance (G)
➢ Susceptance (B)
➢ Admittance (Y)

Figure 3.12: Complex permeability measurement by Wayne Kerr Precision Impedance Analyzer

3.8.2 Permeability Measurement

From the frequency dependence of complex permeability, evolution of permeability and magnetic loss component at different stages of ferrite sample as affected by thermal treatment at different temperature was determined using toroids shape sample prepared with insulating Cu wire. The 4192 LF Impedance Analyzer directly measures the value of inductance, L and loss factor $\qquad$ $D = \tan\delta$ $\qquad$ (3.8)

From inductance the value of real part of complex permeability, μ' can be obtained by

using the relation $\qquad$ $\mu' = \dfrac{L}{L_0}$ $\qquad$ (3.9)

Where L is the inductance of the toroid and L_o is the inductance of the coil of same geometric

shape in vacuum, Lois determined by using the relation, $L_0 = \dfrac{\mu_0 N^2 S}{\pi \bar{d}}$ $\qquad$ (3.10)

Here $\mu_o$is the permeability of the vacuum, N is the number of turns (here N = 5), S is the cross-sectional area of the toroid shaped sample, S = dh, where, $d = \dfrac{d_1 \sim d_2}{2}$ $\bar{d}$ is the average diameter

45

of the toroid sample given as $\bar{d} = \dfrac{d_1 + d_2}{2}$, Where, d_1 and d_2 are the inner and outer diameter of

the toroid samples. Quality Factor $\qquad\qquad Q = \dfrac{1}{\tan \delta_M}$ $\qquad\qquad$ (3.11)

And relative quality factor $\qquad\qquad RQF = \dfrac{\mu'}{\tan \delta_M}$ $\qquad\qquad$ (3.12)

3.9   Dielectric Properties

Ceramics are mostly covalently bonded material hence electrically non conductive or insulator. Importance of particular property depends on the application demand. For instance, dielectric strength is an important parameter for application of ceramic as insulators used in power transmission line, load bearing general insulators, in house hold appliances etc. In this kind of applications where frequency do not exceed 1kHz, the break down strength, measured in kV/cm, together with mechanical strength are important factors. The dielectric constant (ε') or loss factor (ε'') does not matter much. On the other hand, for capacitors and electronics application just the opposite required. The values of ε' and ε'' are of prime importance, not only their room temperature values but also as function of frequency. These are intrinsic properties of material; especially of polycrystalline ceramic can be modified by doping, micro structural variation.

3.9.1 Dielectric Constant

Dielectric constant measurements were done by using Wayne Kerr Impedance Analyzer 6500B. The overall dielectric constant (ε') of an insulator material as given by the relation:

$$D = \varepsilon_0 E = \varepsilon_0 \varepsilon' E \qquad\qquad (3.13)$$

D represents the electric displacement, E the electric field in the dielectric, ε' the dielectric constant and ε_0 permittivity of the vacuum. The dielectric constant ε' is an intrinsic property of a material and a measure of the ability of the material to store electric charge relative to vacuum. It is measured directly from the capacitance of a capacitor in which the material is used as electrode separator or dielectric. The capacitive cell, the dielectric constant (ε'), total charge (q) and capacitance C can be developed as follows:

$$\varepsilon' = \frac{D}{\varepsilon_0 E} = \frac{\dfrac{Q}{A}}{\dfrac{\varepsilon_0 V}{d}} \tag{3.14}$$

$$\therefore Q = \frac{\varepsilon_0 \varepsilon' A V}{d} = CV \tag{3.15}$$

Where
$$C = \frac{\varepsilon_0 \varepsilon' A}{d} \tag{3.16}$$

Here A represents the area of the capacitive cell, d its thickness, C is the capacitance of the material, V the voltage across the cell and $\varepsilon_0 \left(\dfrac{F}{m} \right)$ the material permittivity in vacuum. Thus ε' represents the ratio of the permittivity or charge storage capacity relative to air or vacuum as dielectric. $\varepsilon' = \dfrac{cd}{\varepsilon_o A}$, where c is the capacitance of the pellet in Farad, d the thickens of the pellet in meter, A the cross-sectional area of the flat surface of the pellet in m^2 and ε_o the constant of permittivity for free space. Dielectric measurement as a function of frequency in the range 100Hz-120MHz at room temperature were carried out by using Wayne Kerr Impedance Analyzer 6500B in conjunction with a laboratory made furnace which maintain the desired temperature with the help of a temperature controller.

3.9.2 Dielectric Loss

Dielectric loss often attributed to ion migration, ion vibration & deformation and electric polarization. Ion migration is particularly important and strongly affected by temperature and frequency. The losses due to ion migration increase at low frequency and the temperature increases. By definition, $tan\delta = \frac{\varepsilon''}{\varepsilon'}$ (3.18)
The imaginary part of dielectric constant (ε'') of the sample was calculated using relation: $\varepsilon'' = \varepsilon'$ tanδ; where tanδ is the dielectric loss tangent.

3.10 Vibrating Sample Magnetometer (VSM)

A vibrating Sample Magnetometer (VSM) is a scientific instrument to measure the magnetization of a sample under an external magnetic field. It operates on the Faraday's low of induction. The working principle of VSM is the measurement of the electromotive force induced by a magnetic sample when it is vibrated at a constant frequency in the presence of a static and

uniform magnetic field. In a VSM, a sample is placed within a uniform magnetic field H which induces a magnetization M in the sample. It is then vibrated sinusoidally, which creates a corresponding vibration of the magnetic flux in the pick-up coils nearby and induces a sinusoidal voltage.
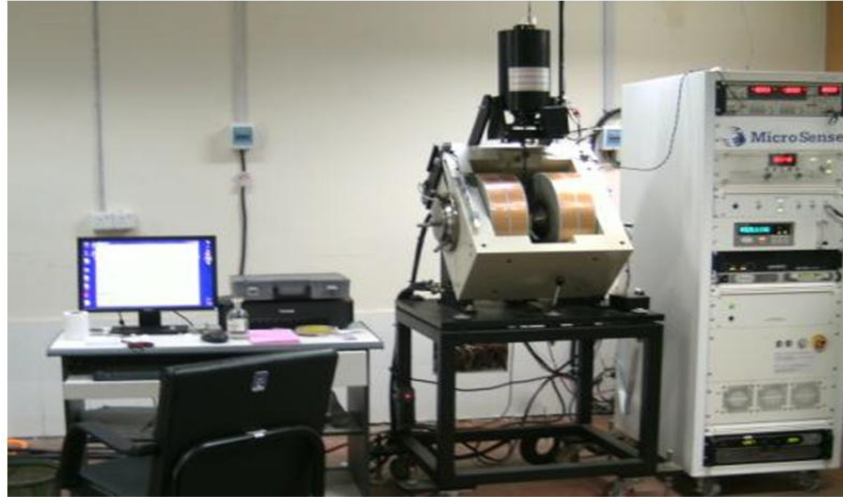
Figure 3.13: Vibrating Sample Magnetometer

The amplitude of the ac voltage is proportional to the samples magnetic moment and measured by a lock-in amplifier [Forner, 1959].In this study, Microsense VSM model EV7 at Atomic Energy Commission, Dhaka was used to determine the magnetic properties of the samples. A small part of the samples (9 -11 mg) were used and was made to avoid movements inside the sample holder. To understand the ferromagnetic effect, full-cycle hysteresis loops were obtained over a wide range of field from -10 KOe to +10 KOe.

3.11 DC resistivity

Sintered pellet specimens were used to determine resistivity. Electrical conductivity of the samples was studied after silver pasting the two polished surfaces of each pellet as shown in Fig. 3.10. The temperature dependent$\rho_{DC}$from room temperature up to 500K were carried out by using two probe method and was estimated by using the following relation $\rho_{DC} = \frac{R\pi r^2}{l}$ Where R is the resistance, r is the radius and l is the thickness of the samples.
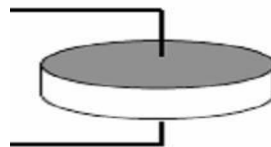
Figure 3.14: Schematic arrangement on the silver pasted pellet sample

48

CHAPTER IV

RESULTS AND DISCUSSION

RESULTS AND DISCUSSION

4.0   Introduction

Rare earth oxides are becoming the promising and potential additives for the improvement of the properties of ferrites. The magnetic and electrical properties can be changed by substitutions various kinds of divalent cations or relatively small amount of rare earth ions [Mondal, 2018; Hossain, 2017; Rezlescu *et al.,* 1997]. Properties are very sensitive to preparation environment such as sintering temperature, time and type of addition of rare earth metal. Present study are addition of small amount of Yttrium (Y) ions to Ni-Zn ferrite samples are changes in their structural, magnetic and transport properties depending upon on amount of Y element used.   In this chapter, structural, magnetic and transport properties of Y doped Ni-Zn ferrites are investigated. The Y substituted polycrystalline $Ni_{0.25}Zn_{0.75}Y_xFe_{2-x}O_4$, [Where x = 0.00, 0.02, 0.04, 0.06 and 0.08] have been prepared by standard solid state reaction technique. XRD patterns of Ni-Zn confirm single phase and formation of cubic structure. The magnetic properties such as complex permeability of the ferrites investigated in the frequency range (1 KHz to 120 MHz) by Wayne Kerr Impedance Analyzer. Surface morphology was measured by SEM (model JEOL JSM 7600F) and hysteresis loop was analyzed by VSM. Dielectric properties, DC resistivity and other electrical properties of the samples are studied.

4.1   X-Ray Diffraction Analysis of $Ni_{0.25}Zn_{0.75}Y_xFe_{2-x}O_4$ Ferrites

XRD analysis is a useful way to get the structural information of a material to evaluate the various phases of the synthesized ferrites as well as their unit cell parameters. To study the structural view of Y doped Ni-Zn ferrites are used Philips X'pert PRO X-ray diffraction using Cu-K_α radiation (λ = 1.5418 Å) in the range of 2θ = 20° to 65° in steps of 0.02°. For XRD analysis is used powder sample of $Ni_{0.25}Zn_{0.75}Y_xFe_{2-x}O_4$ ferrites sintered at 1150°C for 3 hours.

4.1.1 Phase Analysis

The phase formation behavior of $Ni_{0.25}Zn_{0.75}Fe_2O_4$ ferrites sintered at 1150°C for 3 hours are studied by XRD. All this samples show good crystallization with well defined diffraction lines are without doped Y in Ni-Zn ferrites. The structural view or the various phases of Y doped Ni-Zn ferrites were confirmed from XRD analysis. Figure 4.1 shows the X-ray diffraction

patterns of $Ni_{0.25}Zn_{0.75}Y_xFe_{2-x}O_4$ [x = 0.00, 0.02, 0.04, 0.06 and 0.08] ferrites sintered at 1150°C for 3 hours. XRD patterns for all the samples are indexed for fcc spinel structure and Bragg planes are shown in the Figure 4.1. The figure shows eight sharp peaks and the peaks can be indexed as (111), (220), (311), (222), (400), (422), (511), and (440). Here, all the miller indices of a peak are either all odd or even, which confirmed that the samples are spinel lattice with cubic structure. This also confirms the homogeneity of the studied samples.
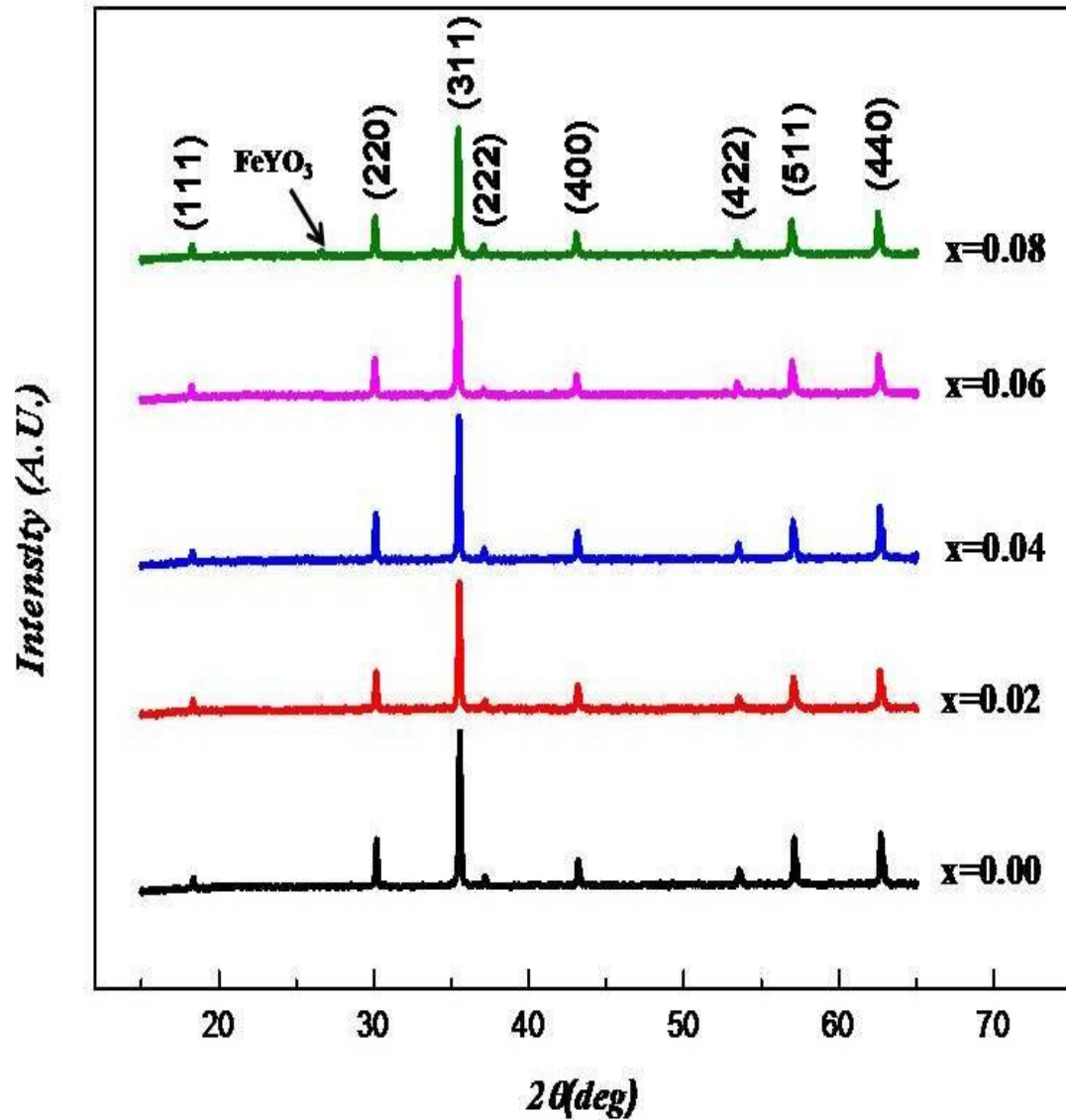

Figure 4.1:   X-ray diffraction spectra of $Ni_{0.25}Zn_{0.75}Y_xFe_{2-x}O_4$, [where x=0.00, 0.02, 0.04, 0.06 and 0.08] ferrites sintered at 1150°C for 3 hours.

All the reflection peaks were identified and indexed in good agreement with the referred database of the International Centre for Diffraction Data (ICDD). All the reflection peaks are identified and indexed in good arrangement, however a very weak reflection peak seen at 2θ is around 26° is more prominent indicated by the arrow is identified $YFeO_3$ orthoferrite phase. From the X-ray data we calculated the position of any peaks and using Bragg's law ($2d \sin\theta = n\lambda$) and calculating the values of interplanar spacing (d). The position of the X-ray peaks and their corresponding miller indices for the studied samples investigated are given in Table 4.1.

Table 4.1: Position of the X-ray peaks and corresponding miller indices for $Ni_{0.25}Zn_{0.75}Y_xFe_{2-x}O_4$ [Where x=0.00, 0.02, 0.04, 0.06 and 0.08] ferrites.

Content	Miller indices of the X-ray peaks and their position 2θ in degree							
	(111)	(220)	(311)	(222)	(400)	(422)	(511)	(440)
X=0.00	18.37	30.19	35.55	37.17	43.19	53.24	57.11	62.17
X=0.02	18.33	30.15	35.51	37.19	43.17	51.51	57.05	62.65
X=0.04	18.29	30.13	35.49	37.13	43.13	53.51	57.05	62.65
X=0.06	18.25	30.07	35.43	37.05	43.09	53.44	56.97	62.59
X=0.08	18.29	30.09	35.45	37.05	43.06	53.43	56.95	62.53

4.1.2 Lattice Parameters

The values of lattice parameters have been determined from each plane of XRD pattern using Nelson Relay function in equation 3.4. The lattice parameters 'a' are plotted against the Nelson Relay function, F (θ) shown in Figure 4.2 for Y content is x. The values of lattice parameters for various $Ni_{0.25}Zn_{0.75}Y_xFe_{2-x}O_4$ ferrites are listed in Table 4.2. This increase in lattice constant can be explained in the basis of ionic radii. The ionic radii of the cations used in $Ni_{0.25}Zn_{0.75}Y_xFe_{2-x}O_4$ are Ni^{2+}(0.7 Å), Zn^{2+}(0.82 Å), Y^{3+} (0.9Å) and Fe^{3+} (0.64Å). The variation of the lattice parameter 'a_0' as a function of Y^{3+} content (x) in the lattice. Figure 4.3 shows the dependence of the lattice parameter 'a_0' on the Y^{3+} content.
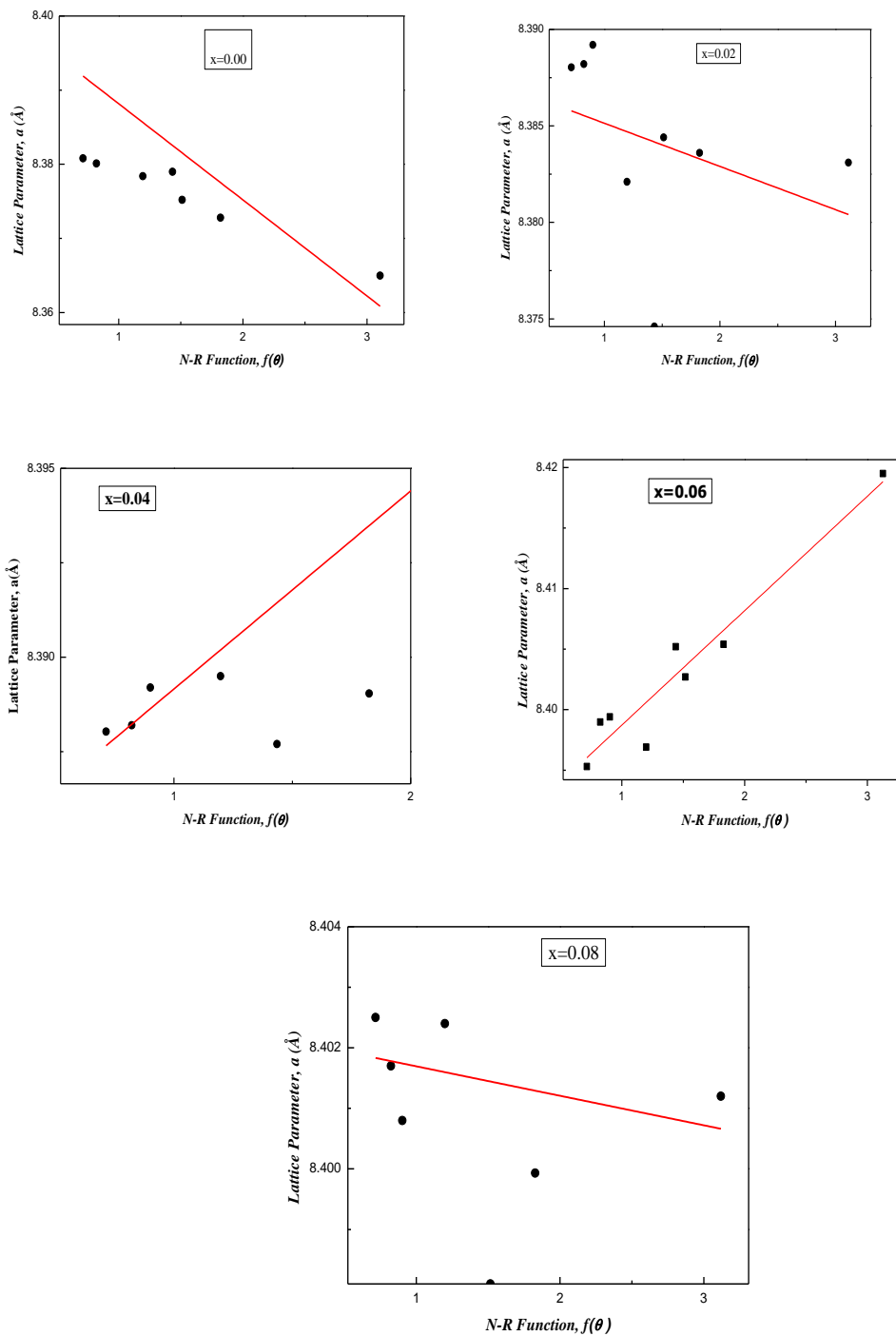
Figure 4.2: Variation of lattice parameter 'a' with N-R function and determination of exact lattice parameter of $Ni_{0.25}Zn_{0.75}Y_xFe_{2-x}O_4$ ferrites.

The lattice parameter increases at x = 0.02, 0.04 and 0.06 due to replacement of Fe^{3+} ions (radius = 0.64Å) by the larger Y^{3+} ions (radius = 0.90Å) in the octahedral sites. It is known that the replacement of cations by larger ones in the spinel lattice causes an increase in the lattice parameter. The slight decrease a_0 for x = 0.08 is probably due to a distortion in the spinel lattice because of the relatively large radius of Y^{3+} ions. This is evidence by the appearance of the minor $FeYO_3$ phase at x = 0.08. in Table 4.2. Table 4.2 shows a increase in lattice constant (a_0) is observed with the increasing Y content in the lattice. This indicates that the present system obeys the Vegard's law [Vegard's, 1921] partially.
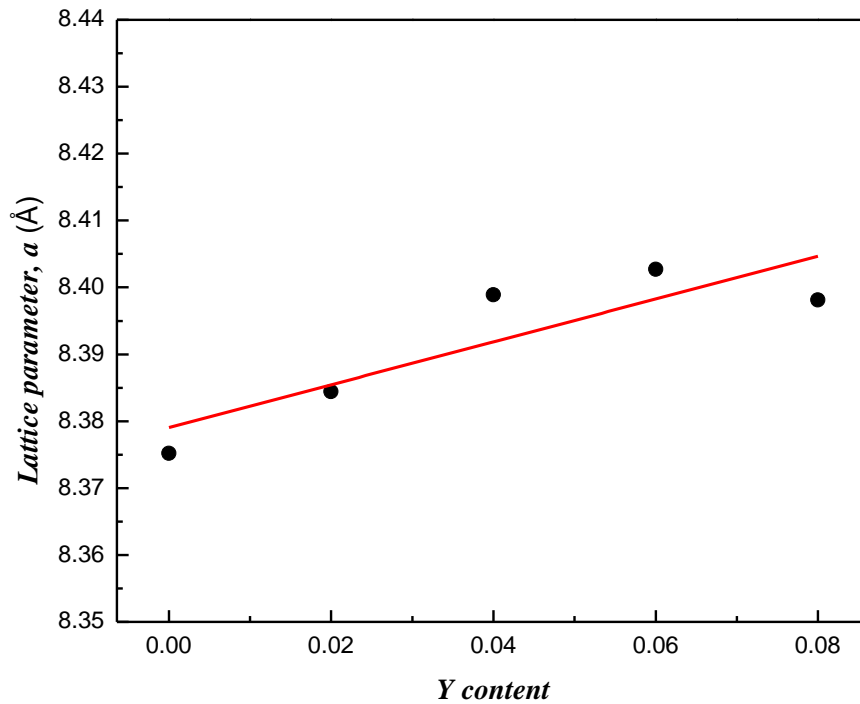
Figure 4.3: Variation of lattice parameters with the increase of Y content.

4.1.3 Density and Porosity

Density of ferrite samples plays an important role in the determination of magnetic and electric properties. It is well known that high permeability could be achieved by increasing the density of the ferrites. The X-ray density calculated from the determined lattice parameter and bulk density measured from the ratio of mass and volume of all the $Ni_{0.25}Zn_{0.75}Y_xFe_{2-x}O_4$ ferrite

samples. The calculated values of the X-ray density (ρ_x), bulk density (ρ_B) and porosity (P %) of the present ferrites are listed in Table 4.2. The X-ray density or theoretical density ρ_x is found to be increased from 5.41 to 5.43 g/cm^3 with the increase in Y^{3+} substitution. The net result is that the composition has non-stoichimetry excess Ni and Zn. This non-stoichimetric excess Ni and Zn are used for low temperature liquid phase sintering of the ferrites [Fujimoto, 1994]. For this reason, the densification increased with Y substitution.

Table 4.2: Data of the lattice parameter (a), X-ray density (ρ_x), bulk density (ρ_B), porosity (P%) of $Ni_{0.25}Zn_{0.75}Y_xFe_{2-x}O_4$, [Where x=0.00, 0.02, 0.04, 0.06 and 0.08] ferrites sintered at 1150°C for 3 hours.

Content	a (Å)	ρ_x (gm/cm^3)	ρ_B (gm/cm^3)	Porosity (%)
X= 0.00	8.375	5.41	4.90	9.55
X= 0.02	8.384	5.41	4.75	12.20
X= 0.04	8.399	5.40	4.82	10.60
X= 0.06	8.403	5.40	4.91	9.10
X= 0.08	8.398	5.43	4.86	10.50

Here the X-ray density is related to the molecular weight (M) and lattice constant (a).The increase in X-ray density might be due to the greater atomic mass of Y^{3+} (88.90 amu) than that of Fe^{3+} (55.85 amu). It is observed that bulk density is lower than the X-ray density shown in Figure 4.4. This may be due to the existence of pores which were formed and developed during the sample preparation or sintering process. The bulk density decreases with increasing rare earth ion Y^{3+} and the X-ray density increases with increasing Y-content.

It is observed that porosity increases monotonically with increasing Y^{3+} content. It was difficult to remove these closed porosities completely due to the evaporation of constituents specially Zn. This may be due to the porosity or voids into the samples are not considered in the X-ray density. In this case imaginary mass is considered instead of real mass. On the other hand, in the case of bulk density real mass and dimensions are taken. It is known that the porosity of the samples come from two sources, intragranular porosity and intergranular porosity. The intergranular porosity mainly depends on the grain size [Yang *et al.,* 2006]. The porosity which

is intrinsic for any oxide material plays an important role in the deciding the magnetic and electrical properties due to pore spaces.
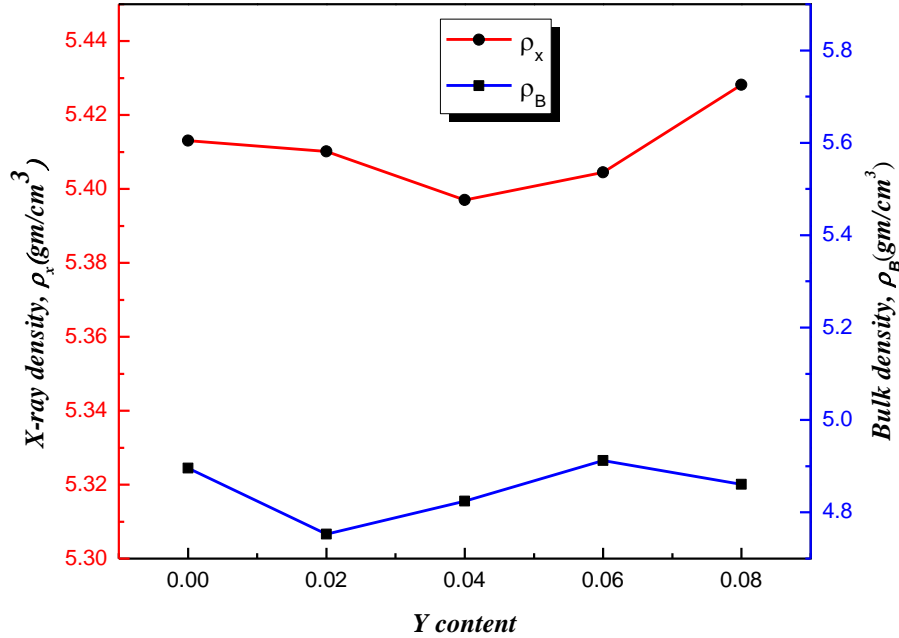
Figure 4.4: Variation of bulk density and X-ray density as a function of Y content

The enhancement of bulk density is due to activated diffusion process triggered by the excess vacancies created by Fe^{3+} deficiency. It may be also be mentioned that reduction Fe^{2+} due to Fe^{3+} deficiency is expected to increase the resistivity of the samples. This density plays an important role on the magnetic properties especially on the structure sensitive property such as permeability and flux density. At higher sintering temperatures the density is decreased because the intragranular porosity is increased resulting from discontinuous grain growth.

4.2   Microstructures of $Ni_{0.25}Zn_{0.75}Y_xFe_{2-x}O_4$ Ferrites

Structural, magnetic and electrical properties of ferrites are sensitively depending on the microstructure of the ferrite samples. Microstructure means grain size is an important parameter affecting the magnetic properties of ferrites. Grain growth is closely related to the grain boundary mobility.
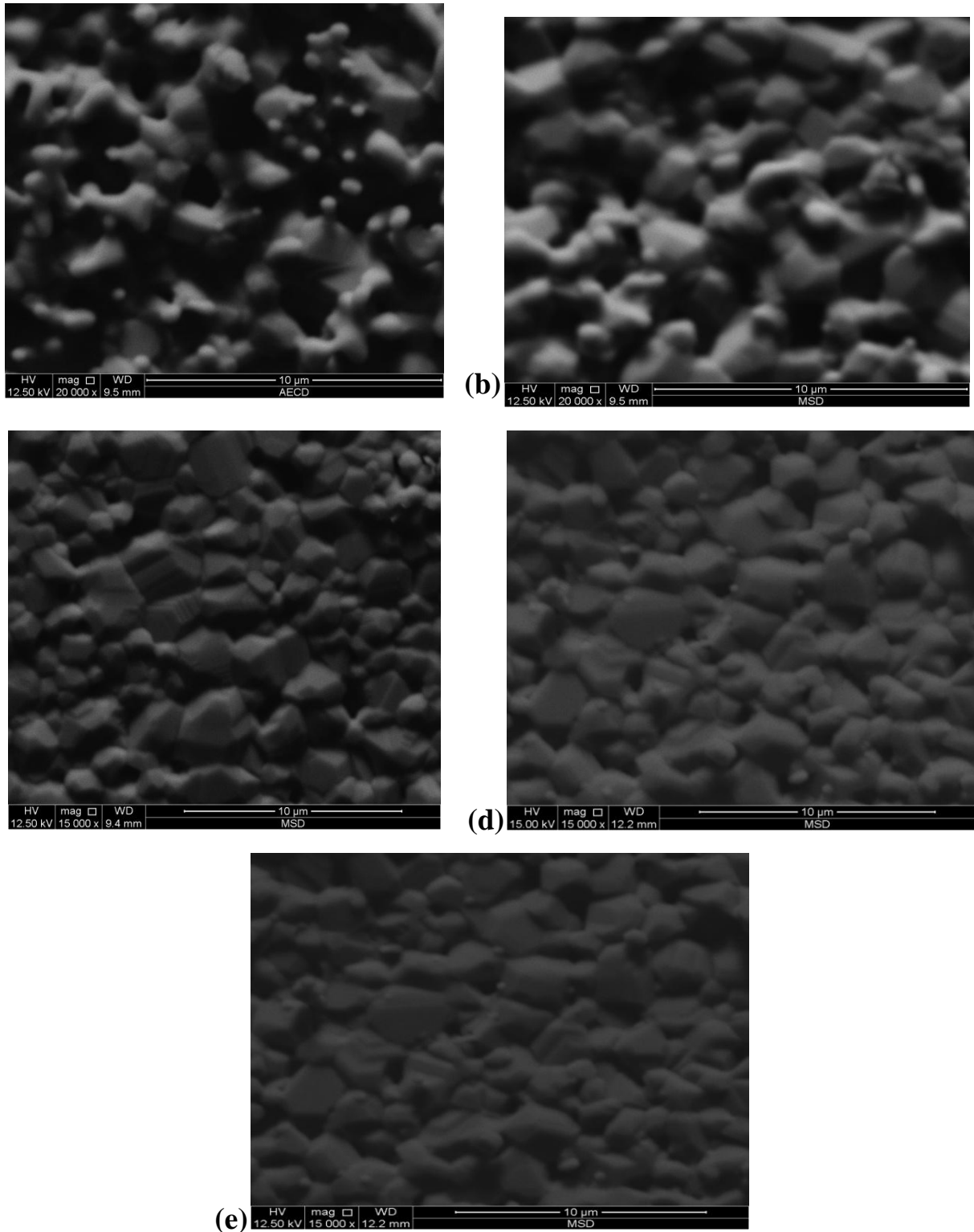
Figure 4.5 (a, b, c, d & e): SEM micrograph of $Ni_{0.25}Zn_{0.75}Y_xFe_{2-x}O_4$, [Where x=0.00, 0.020.04, 0.06 and 0.08] ferrites sintered at 1150°C/3hrs.

Recrystallization and grain growth involve the movement of grain boundaries. Figure 4.5 shows the SEM microstructure of $Ni_{0.25}Zn_{0.75}Y_xFe_{2-x}O_4$ ferrites pellets sintered at 1150°C for 3 hours. The average grain size was calculated using Image J software from the SEM micrograph and has been shown in Table 4.3. From these above figures the average grain size increases gradually with increasing Y content. It occurred due to the fact that sintering of ferrites might be assisted by a liquid phase that drew the particles together due to capillary forces and enabled more densification. It is clear that the microstructure of Ni-Zn-Y ferrite strongly depend on the amount of Y-content in the samples. Figure 4.5 (a) showed the presence of a monophasic homogeneous microstructure without Y content. Y doped specimens shown in figure 4.5 (b, c, d & e) are biphasic homogeneous microstructure constituted of dark ferrite matrix grain and small whitish grain at the grain junction/boundary. The grain size of matrix phase is maximum at 1943nm for x = 0.06. Relatively lower grain size of ferrite matrix at x =0.00 composition shows other doped Y might be due to the grain growth inhibition caused by $YFeO_3$ are clear visible.

Table 4.3: Average grain size for$Ni_{0.25}Zn_{0.75}Y_xFe_{2-x}O_4$ ferrites.

Name of the sample	Contents	Average grain size(nm)
$Ni_{0.25}Zn_{0.75}Fe_2O_4$	X = 0.00	1355
$Ni_{0.25}Zn_{0.75}Y_{0.02}Fe_{1.98}O_4$	X = 0.02	1426
$Ni_{0.25}Zn_{0.75}Y_{0.04}Fe_{1.96}O_4$	X = 0.04	1608
$Ni_{0.25}Zn_{0.75}Y_{0.06}Fe_{1.94}O_4$	X = 0.06	1943
$Ni_{0.25}Zn_{0.75}Y_{0.08}Fe_{1.92}O_4$	X = 0.08	1877

Here the average grain size was estimated in the range from 1355 nm to 1943 nm. The crystal grain growth depends on grain boundaries migrating and larger crystal grains swallowing the small ones. It facilities the grain growth by increasing the rate of cations inter diffusion as a result of its segregation to the grain boundaries [Mendelson, 1969]. The grain growth, being a result of interparticle mass transport, appears to be dominated by the bimodal diffusion mechanism [Gupta and Coble, 1968]. The behavior of grain growth reflects the competition

between the driving force for grain boundary movement and the retarding force that drives the grain boundaries to grow over pores. The driving force of the grain boundary in each grain is homogeneous, the sintered body attains a uniform grain distribution. Abnormal grain growth occurs if this driving force is inhomogeneous. Moreover the strength of the driving force depends upon the diffusivity of individual grains, sintering temperature and porosity.

4.3 Magnetic Properties

4.3.1 Variation of Saturation Magnetization at Room Temperature

The room temperature magnetic hysteresis graphs of $Ni_{0.25}Zn_{0.75}Y_xFe_{2-x}O_4$, [Where x=0.00, 0.02, 0.04, 0.06 and 0.08] ferrites sintered at 1150°C/3hrs has been measured at room temperature up to 10kOe magnetic field (H) and presented in Figure 4.6.

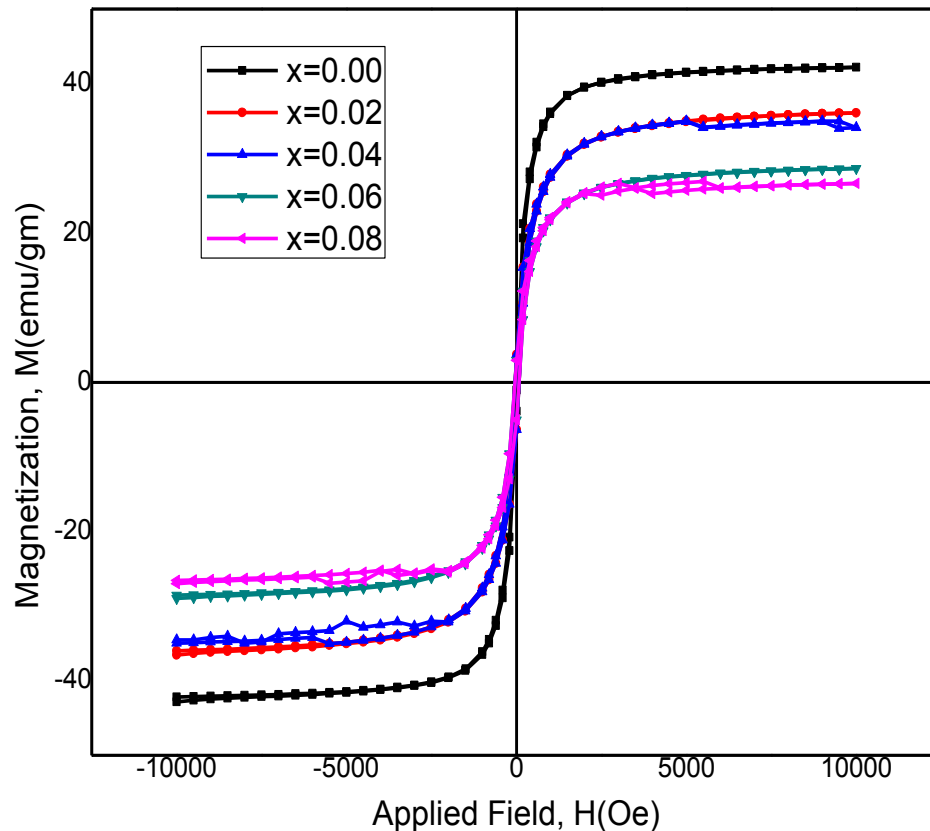Figure 4.6: Variation of magnetization at room temperature as a function of applied field on $Ni_{0.25}Zn_{0.75}Y_xFe_{2-x}O_4$, [Where x=0.00, 0.020.04, 0.06 and 0.08] ferrites sintered at 1150°C/3hrs

All measurable samples exhibit low coercivity values indicating that doped Y and undoped samples being to the family of soft ferrites. These are magnetization curve nature is connected with soft magnetic behavior of Y doped Ni-Zn ferrites. The magnetization (M) of all ferrites increases linearly with increasing the applied magnetic field (H) up to 1.6kOe. After 1.6kOe the applied field M increases slowly and then saturation occurs. All ferrites samples are in ferromagnetic state and get hysteresis loop for $Ni_{0.25}Zn_{0.75}Y_xFe_{2-x}O_4$ system. All hysteresis curves observed that the magnetization process increases sharply at low field (H < 2.5Oe) which corresponds to magnetic domain reorientation that after increases slowly up to saturation due to spin rotation. This magnetization process is connected with soft magnetic behavior of magnetic material. The slow process of magnetization toward the saturation value is connected with the magnetic anisotropy effect. Actual saturation could not be attained even with magnetic field as high as 10 KOe. From the hysteresis loop the saturation magnetization (M_s), coercivity (H_c), remanent magnetization (M_r), magnetic moment were calculated and listed in Table 4.4.

Table 4.4: Saturation magnetization (M_s), coercivity (H_c) and remanent magnetization (M_r) of $Ni_{0.25}Zn_{0.75}Y_xFe_{2-x}O_4$, [where x = 0.00, 0.02, 0.04, 0.06, and 0.08] ferrites sintered at 1150°C holding time 3hours

Content, Y	M_s (emu/gm)	H_c (Oe)	M_r (emu/gm)	M_r/M_s
X= 0.00	41.82	42.17	3.93	0.09
X= 0.02	36.10	35.99	3.68	0.10
X= 0.04	34.73	34.99	3.68	0.11
X= 0.06	28.53	28.55	2.92	0.10
X= 0.08	26.74	26.55	2.92	0.11

The value of M_s has found to be decreases with the increasing of Y^{3+} doped content for measurable all samples. It can be seen here conventionally that, doping accompanies grain growth and that is responsible for the decreases of magnetization due to the decrease of Fe content. There is a large change in the magnetic state due to cation distribution. The superexchange interaction between iron ions in tetrahedral and octahedral sites leads to the ordering in magnetic moment. In decreases M_s with increasing rare earth Y is due to the increase

of resultant sub lattice magnetic moment which can be explained on the basis of Neel's two sub lattice model. Neel [Neel, 1948] considered three types of exchange interactions between unpaired electron of two ions lying in A and B sites. In perfect ferrites, the A - A, B - B and A - B nearest neighbor exchange coupling are normally anti ferromagnetic and the A - B exchange coupling is usually heavily predominant. The net magnetization is therefore the difference between the magnetic moments of B and A sub lattices, i.e. $M = M_B - M_A$ and will normally be parallel to the B-sub lattice magnetization because the number of cations on B-sites is twice the number of cations on A-sites. The magnetization of each composition depends on the distribution of Fe^{3+} ions between the two sub lattices A and B, where the Ni^{2+} and Zn^{2+} ions are non magnetic. It is mentioned that $Ni_{0.60}Zn_{0.40-x}Y_xFe_{2-x}O_4$ ferrites, where Ni^{2+} and Fe^{3+} ions are located on B-sites and Zn^{2+}ions show a strong preference for tetrahedral A-site due to its electronic configuration. Similarly, the rare earth ions Y could not enter into the B site and accumulate on the grain boundary.

Figure 4.7 (a) shown in below delineates the zoomed hysteresis characteristic of undoped Ni-Zn ferrite. Here it can be seen that, the undoped samples exhibit soft ferrimagnetic behavior where the magnetic domains align in an antiparallel direction with unequal magnetudes of magnetic moment. The saturation magnetization (M_s), Remanent magnetization (M_r) and coercivity (H_c) have very small values are 41.82emu/gm, 42.17Oe and 3.93emu/gm respectively.
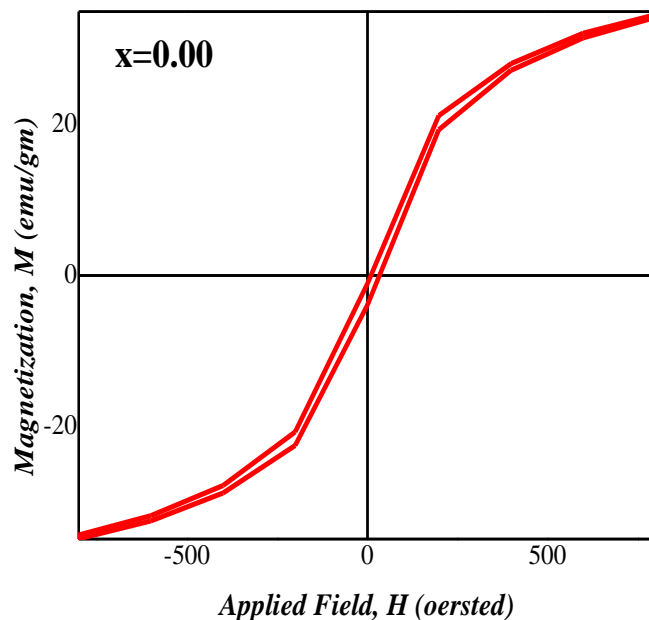
Figure 4.7(a) : Hysteresis loop for undoped $Ni_{0.25}Zn_{0.75}Fe_2O_4$ ferrite
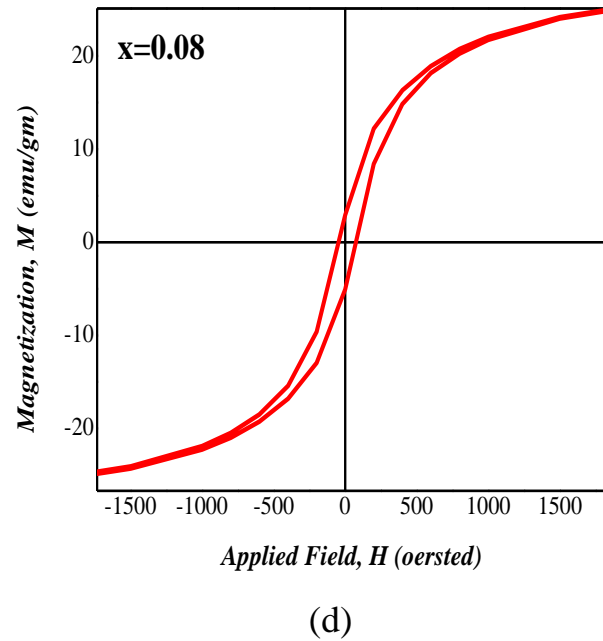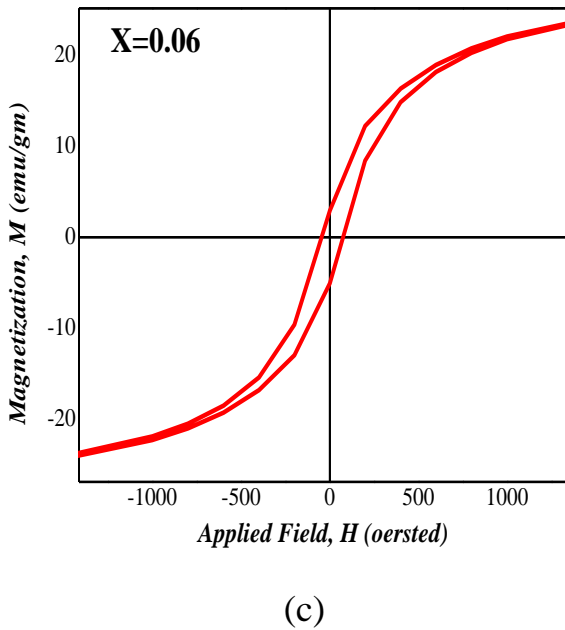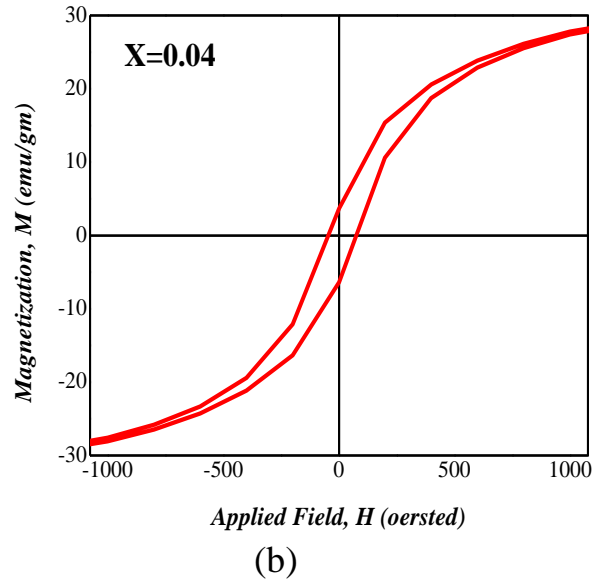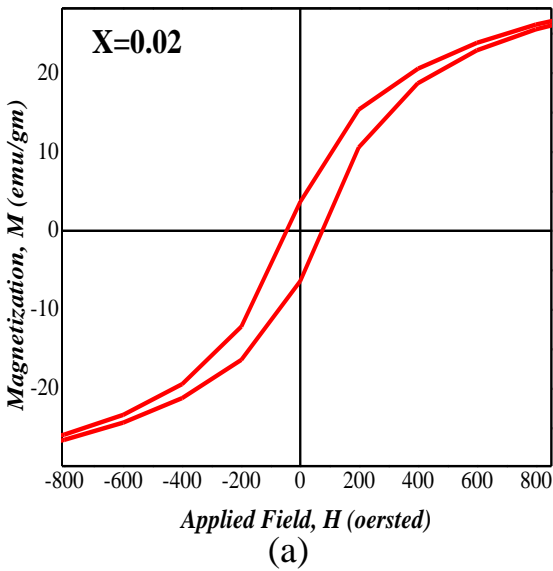
Figure 4.8 (a, b, c and d) :   Hysteresis loop for $Ni_{0.25}Zn_{0.75}Y_xFe_{2-x}O_4$, [where x = 0.00, 0.02, 0.04, 0.06, and 0.08] ferrites

The above figures 4.8 (a, b, c and d) shows the hysteresis behavior of Y doped Ni-Zn ferrite for all concentrations of x (0.02, 0.04, 0.06 and 0.08). Here, all the graphs also showing the ferrimagnetic behavior as like as the undoped samples. It can be seen here that, saturation magnetization and specially coercivity decreases significantly with increasing of Y content.

These are indicating the ferrimagnetic to superparamagnetic transition behavior of Ni-Zn ferrite with the increasing of Y content. The hysteresis loops do not show any noticeable hysteresis effect. All samples exhibited low coercivity in the range of 25 to 45Oe values indicating that all the samples belong to the family of soft ferrites. The value of M_s were found to be decreases with the increasing of Y^{3+} doped content for all the samples. The decrease in M_s can be explained by the cation distribution in which Y^{3+} ions can convert some of Fe^{2+} to Fe^{3+} in B-sites. The magnetic moment of Fe^{2+} is less than that of the Fe^{3+}, therefore magnetic moment (μ_B) as well as M_s as shown in Table 4.4. Here the value of effective magnetic moment and radii of Y^{3+} ions are responsible for decreasing M_s. We know that Fe^{3+}-Fe^{3+} interaction is very strong, when we doped Y^{3+} ion with replacing Fe^{3+} ion then the interaction between Fe^{3+}-Fe^{3+} decreased. For this reason the M_s decreases with the increasing of the Y^{3+} doped content.

The value of H_c and M_r of nominal composition at x = 0.00 has higher value than that of the samples doped by Y in Ni-Zn ferrites. This might be due to better density and higher permeability of the Y-doped Ni-Zn ferrite. The H_c and M_r were found in Table 4.4 to be gradually decreased with increasing of Y content. These are the consequences of gradual decrease of the magnetic iron (Fe) quantity from the samples as well as the replacement of that quantity of Y with the Fe. The variation of remanent ratio (M_r/M_s) and $H_c$with respect to the addition of Y content are graphically shown below for better convenience.
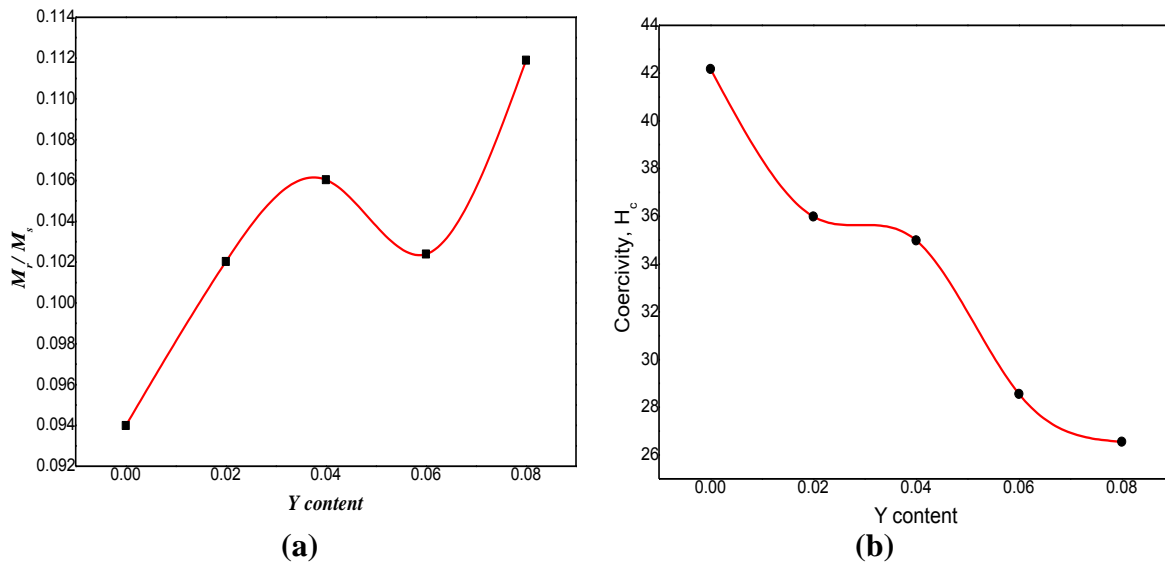

(a)   (b)

Figure 4.9:   (a) M_r/M_s versus Y content and (b) H_c versus Y content in $Ni_{0.25}Zn_{0.75}Y_xFe_{2-x}O_4$, ferrites sintered at 1150°C holding time 3hours.

4.3.2 Frequency Dependence of Complex Permeability

The complex permeability is given by $\mu = \mu' - i\mu''$, where μ' and μ" are the real and imaginary part of the complex permeability respectively. Here μ' describes the stored energy expressing the component of magnetic induction B in phase and μ" describes the dissipation of energy expressing the component 90° out of phase of B with alternating magnetic field. The μ' of ferrites depends on many factors like reversible domain wall displacement, the amount and the type of dopant ions and intragranular porosity etc [Haque *et al*., 2008; Murthy, 2001]. μ' of polycrystalline ferrite is related to two magnetizing mechanisms: domain wall motion and spin rotation [Hu Jun and Yan Mi, 2005; Tsutaoka *et* al., 1995; Wohlfarth, 1980]. Ni-Zn ferrites are several studied and found a linear relationship between μ' and dopant ions [Globus *et al* , 1971].

For all the samples of $Ni_{0.25}Zn_{0.75}Y_xFe_{2-x}O_4$, ferrites are used conventional technique based on the determination of the complex impedance of circuit loaded with toroid shaped sample. With the help of Wayne Kerr Impedance Analyzer we collected 800 data point for initial permeability at different frequency range from 1KHz to 120MHz. Figure 4.10 shows the variation on real part of complex permeability μ' spectra as a function of frequency range 1kHz to 120MHz of $Ni_{0.25}Zn_{0.75}Y_xFe_{2-x}O_4$ ferrites for different values of x at sintering temperature 1150^oC holding time 3 hrs. Among these data some of the values of initial permeability at different frequency range are listed in Table 4.5. For avoiding the noise peak we only took these values of initial permeability at different frequency range from 1MHz to 120MHz. It is seen that μ' remains almost constant until very high frequency (around 60MHz) and then drops rapidly. The fairly constant μ' values over a wide range of frequency region are known as the zone of utility because it demonstrates the compositional stability and quality of the prepared samples. Here the initial permeability remains stable for a long frequency range due to hopping of electron between Fe^{2+} and Fe^{3+}. It could be observed that the initial permeability increases significantly with substitution of Y content. At low frequencies, a ferrite inductor is a low loss constant self inductor μ' is stable and the core is mostly inductive, rejecting the electromagnetic interference (EMI) signal of source [Snelling, 1988; Khan *et al.,* 2013]. From the Figure 4.9 the ranges of operating frequency up to 30MHz at constant frequency all the doped samples wider than the other ferrite sample and quality of the doped Y^{3+} in Ni-Zn ferrites. The substitution of ferromagnetic Fe^{3+} by diamagnetic Y^{3+} in the spinel is not metal for increasing permeability

significant. In this present case Y^{3+} incorporation into the lattice is very small and hence slight enhanced permeability with increasing Y^{3+} ions due to incorporation.

Figure 4.10: Frequency dependent initial permeability of $Ni_{0.25}Zn_{0.75}Y_xFe_{2-x}O_4$, [Where x=0.00, 0.02, 0.04, 0.06 and 0.08] ferrites sintered at 1150°C for 3 hours.

Table 4.5: Values of initial permeability at different frequency range for $Ni_{0.25}Zn_{0.75}Y_xFe_{2-x}O_4$, [Where x=0.00, 0.02, 0.04, 0.06 and 0.08] ferrites.

Y Content	μ' at 100Hz	μ' at 10KHz	μ' at 100KHz	μ' at 1MHz	μ' at 10MHz	μ' at 100MHz
X = 0.00	16	17	17	17	16	14
X = 0.02	15	17	17	17	16	15
X = 0.04	17	18	18	18	17	15
X = 0.06	26	26	26	26	25	20
X = 0.08	27	27	27	26	25	19

The initial permeability of $Ni_{0.25}Zn_{0.75}Y_xFe_{2-x}O_4$ ferrite materials are also depend on many factors like reversible domain wall displacement, domain wall bulging as well as microstructural features, average grain size, intra granular porosity, etc [Smit and Wijn, 1959]. When frequency is low then we get high permeability and when frequency is high then gets permeability is low. Thus, an effective limit of product of frequency and permeability can be established.
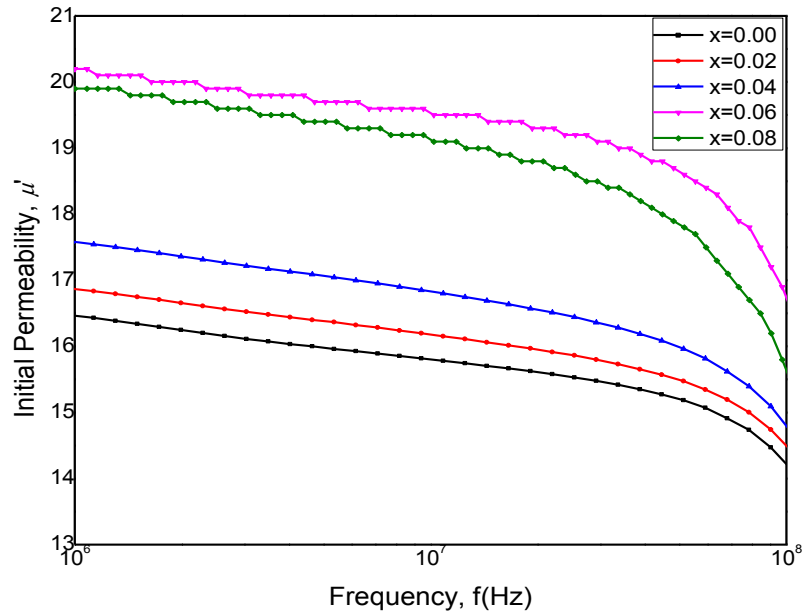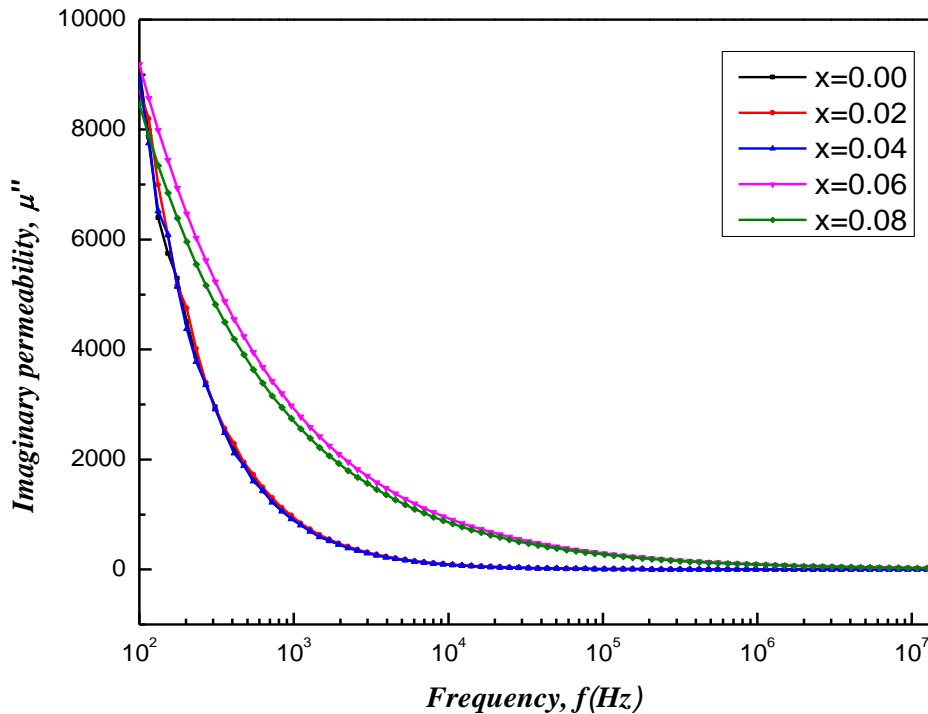

Figure 4.11:   Frequency dependent imaginary permeability of $Ni_{0.25}Zn_{0.75}Y_xFe_{2-x}O_4$, [Where x=0.00, 0.02, 0.04, 0.06 and 0.08] ferrites sintered at 1150°C/3 hour

Figure 4.11 shows the imaginary permeability (μ'') initially high at low frequency zone all the samples and then decreases with increasing frequency almost μ'' constant high frequency range. The grain growth increases with increasing Y content diminishes the grain boundary, thereby the domain walls can not move easily leads to lower permeability. The decrease in imaginary permeability implies onset of ferromagnetic resonance [Globus *et al.,* 1977]. Also

65

during grain growth pores become fewer, which act as independents to domain wall motion due to pinning wall. At high frequencies at constant μ'' parameters become more significant, the inductors show high impedance and become resistive and dissipate interfacing signals rather than reflecting this source.

4.3.3 Frequency Dependence of Loss Tangent

Loss factor is an important parameter in a soft ferromagnetic material, since the amount of energy wasted on process other than magnetization can prevent the AC applications of a given material. The ratio of μ'' and μ' is equal $\tan\delta$ representing the losses in the material are a measure of the inefficiency of the magnetic system. The variation of loss factor, $\tan\delta$ ($= \mu''/\mu'$) with frequency for all samples has been studied. Figure 4.12 shows the variation of loss factor ($\tan\delta$) with frequency for various $Ni_{0.25}Zn_{0.75}Y_xFe_{2-x}O_4$, samples sintered at 1150°C holding time 3 hours. The magnetic losses, which cause the phase shift, can be split up into three components: hysteresis losses, eddy current losses and residual losses. This gives the formula $\tan\delta m = \tan\delta_h + \tan\delta_e + \tan\delta_r$. As μ' is the initial permeability which is measured in presence of low applied magnetic field, therefore, hysteresis losses vanish at very low field strengths.

Thus at low field the remaining magnetic losses are due to eddy current losses and residual losses. Residual losses are independent of frequency. Eddy current losses increase with frequency and are negligible at very low frequency. Eddy current loss can be expressed energy loss per unit volume and is the resistivity [Valenzuela, 1994]. To keep the eddy current losses constant as frequency is increased; the resistivity of the material chosen must increase as the square of frequency. Eddy currents are not problem in the Ni-Zn ferrites until higher frequencies are encountered because they have very high resistivity about $10^5\Omega$-cm to $10^8\Omega$-cm [Brailsford, 1996]. The ferrite microstructure is assumed to consist of grains of low resistivity separated by grain boundaries of high resistivity. Thicker grain boundaries are preferred to increase the resistance

It is clear from the Figure 4.12 that the value of $\tan\delta$ is less frequency dependent in the frequency range from 1kHz to 100MHz. Therefore, it is concluded that the synthesized composites have excellent performance in a wide frequency range and can be used for MLCF application, such as embedded inductors or embedded capacitors.

At lower frequencies, a decrease in magnetic loss is observed. The lag of domain wall motion with respect to the applied magnetic field is responsible for magnetic loss and this is accredited to lattice imperfections [Cullity, 1972].

Figure 4.12:   Frequency dependent loss factor of $Ni_{0.25}Zn_{0.75}Y_xFe_{2-x}O_4$, [Where x=0.00, 0.02, 0.04, 0.06 and 0.08] ferrites sintered at 1150°C for 3 hour

4.3.4 Frequency Dependence of Quality Factor

The frequency dependence of $Ni_{0.25}Zn_{0.75}Y_xFe_{2-x}O_4$ ferrites sintered at 1150^0C/3hrs have been calculated from the relation $Q = 1/\tan\delta$; where tanδ is the loss factor is used to measure the merit of the magnetic materials. Figure 4.13 shows the frequency dependence quality factor (Q-factor) of sample are $Ni_{0.25}Zn_{0.75}Y_xFe_{2-x}O_4$ sintered at 1150^0C for 3 hours. Q-factor increases with an increase of frequency showing a peak and then decreases with further increase of frequencies. It is seen that Q-factor again deteriorates beyond 1MHz for Y i.e. the loss tangent is minimum around 1 to 4MHz. The loss is due to the loss of domain wall motion with respect to the applied alternating magnetic field and is attributed to various domain defects [Overshott K.,

1981] which include non- uniform and non-repetitive domain wall motion, domain wall bowing, and localized variation of flux density, nucleation and annihilation of domain walls.

The peak corresponding to maxima in Q-factor shifts in 10 MHz frequency range as Y content increases and it has an increasing tendency in the higher frequency range. Sample with x = 0.06 possesses the maximum value of Q-factor. The low frequency dispersions are associated with domain wall dynamics [Gorter E. W., 1954] and high frequency to spin rotation. Samples are shown here for a better understanding for the merit of the prepared materials for an induction device application. Ni-Zn-Y ferrites have been found to demonstrate reasonably good permeability at room temperature covering stable wide range of frequency indicating the possibilities for applications as high frequency up to several MHz induction and/or core materials. These means that Ni-Zn-Y ferrite materials are suitable for high frequency applications with stable permeability range.
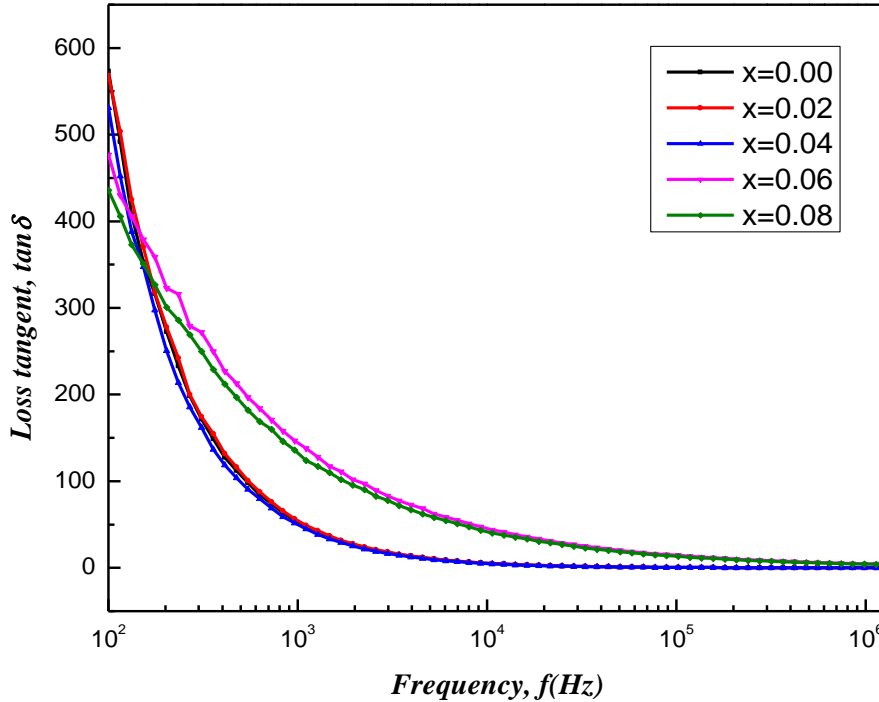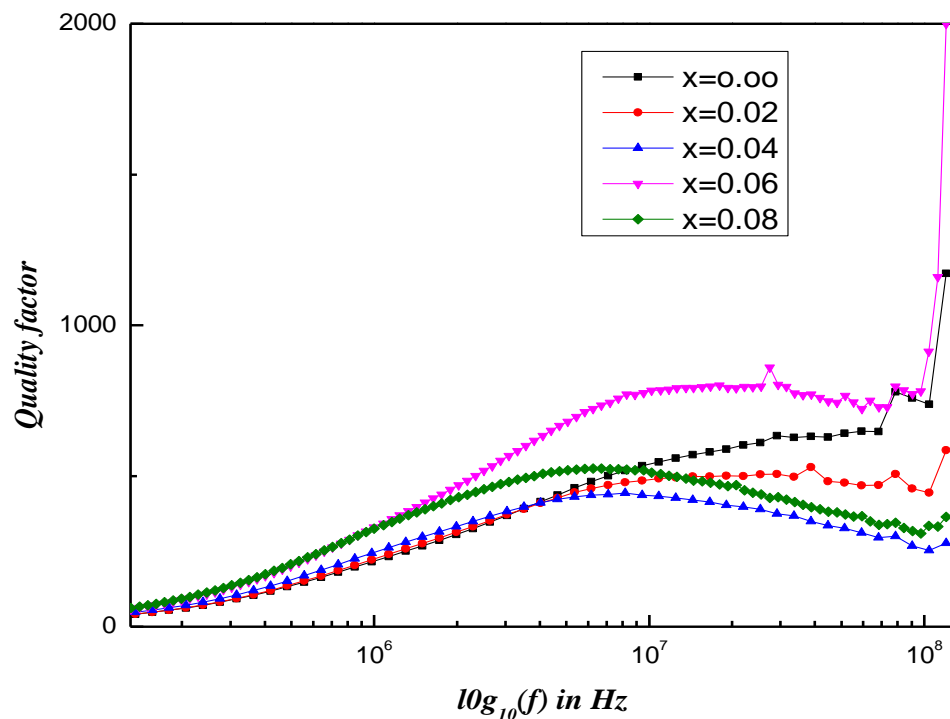

Figure 4.13:   Frequency dependent loss factor of $Ni_{0.25}Zn_{0.75}Y_xFe_{2-x}O_4$, [Where x=0.00, 0.02, 0.04, 0.06 and 0.08] ferrites sintered at 1150°C for 3 hours.

4.4   Frequency Dependent Dielectric Properties

Figure 4.14 shows the variation of dielectric constant, ε' with frequency for different composition of $Ni_{0.25}Zn_{0.75}Y_xFe_{2-x}O_4$ [Where x = 0.00, 0.02, 0.04, 0.06 and 0.08] ferrites sintered at 1150°C/3hrs. Here the dielectric constant was measured over a wide range of frequency from 1 KHz to 120 MHz at room temperature. It can be seen from the Figure 4.14 that the dielectric constant is found to decrease continuously with increasing frequency for all the specimens. The decrease in dielectric constant with increasing frequency is a normal behavior of ferrites, which was observed before Mg-Zn ferrite [Jadhav *et al.,* 1999] and Co-Zn ferrite [Kodama, 1999]. The dielectric dispersion is rapid at lower frequency region and it remains almost independent at high frequency side.
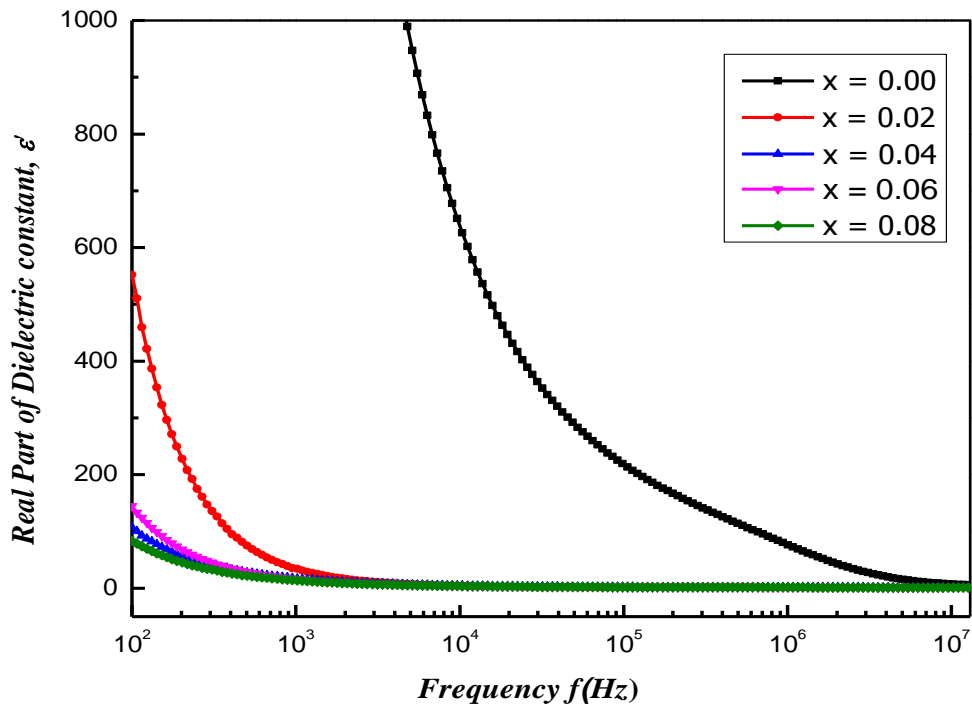

Figure 4.14:   Frequency dependent real part of dielectric constant of $Ni_{0.25}Zn_{0.75}Y_xFe_{2-x}O_4$, [Where x=0.00, 0.02, 0.04, 0.06 and 0.08] ferrites sintered at 1150°C for 3 hours.

The effect of rare earth Y^{3+} substitution into these ferrites has no pronounced effect on the dielectric constant in high frequency, but significantly decreases the dielectric constant in the

low frequency range. The dielectric behavior of ferrites may be explained on the basis of the mechanism of the dielectric polarization process and is similar to that of the conduction process. The electronic $Fe^{2+} \leftrightarrow Fe^{3+}$ gives the local displacement of electrons in the direction of applied electric field, which induces the polarization in ferrites [ZhenxingYue *et al.,* 2001]. The magnitude of exchange depends on the concentration Fe^{2+}/Fe^{3+} in pairs present on B-site for the present ferrite. All the samples have high value of $\varepsilon^{/}$ in the order of 10^5 at low frequencies. This could be explained using Koop's phenomenological theory [Maxwell, 1873; Wanger, 1913] which was based on the Maxwell-Wagner model for the inhomogeneous double layer dielectric structure. The first layer is the fairly well conducting large ferrite grain which is separated by the second thin layer of the poorly conducting grain boundaries. The grain boundaries of the lower conductivity were found to be ferrite at lower frequencies while ferrite grains of high conductivity are effective at high frequency.
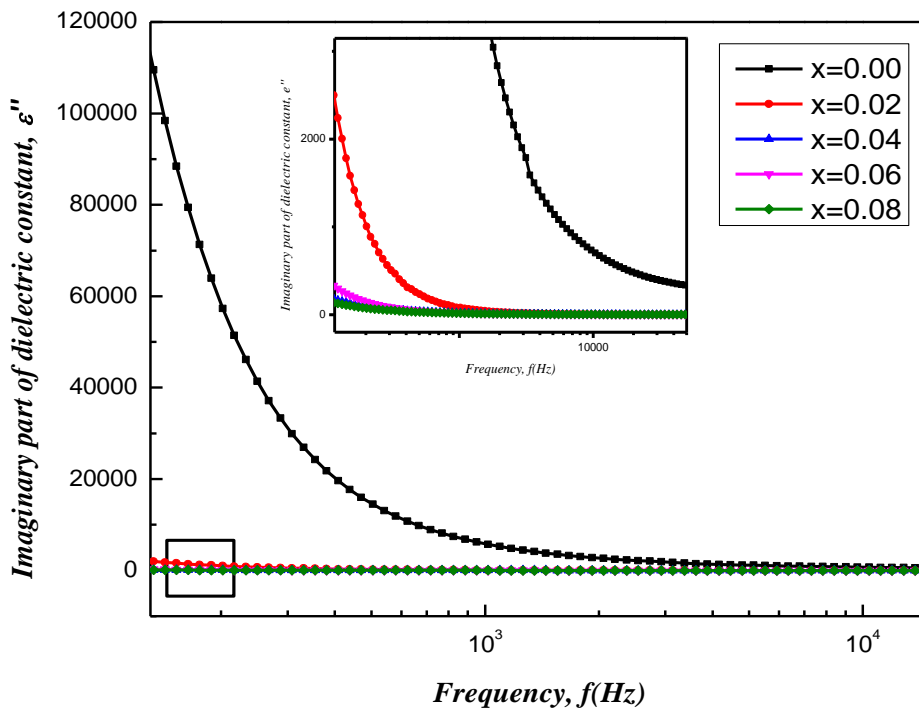
Figure 4.15: Frequency dependent imaginary part of dielectric constant of $Ni_{0.25}Zn_{0.75}Y_xFe_{2-x}O_4$, [Where x=0.00, 0.02, 0.04, 0.06 and 0.08] ferrites sintered at 1150°C for 3 hours

70

The imaginary part of dielectric constant, ε'' was also decreased with increasing frequency as shown in Figure 4.15. At very high frequency the value of ε'' becomes so small that it remains independent of applied frequency. The rapid decrease of ε'' at lower frequencies can also be explained on the basis of space charge polarization. We know that ferrites are made up of well conducting layer of grains followed by poorly conducting layer of grain boundaries. During the exchange process between Fe^{3+} - Fe^{2+} the electrons have to pass through the grains and grain boundary of the dielectric medium. After that the electrons accumulate at grain boundary and produce space charge polarization. At low frequency the grain boundaries are more effective and at high frequency grains are effective. For this reason, grain boundary effect is responsible for decreasing imaginary part of the dielectric constant rapidly at low frequency region. At high frequency the polarization decreased, thus resulting in a decrease in imaginary part of the dielectric constant.
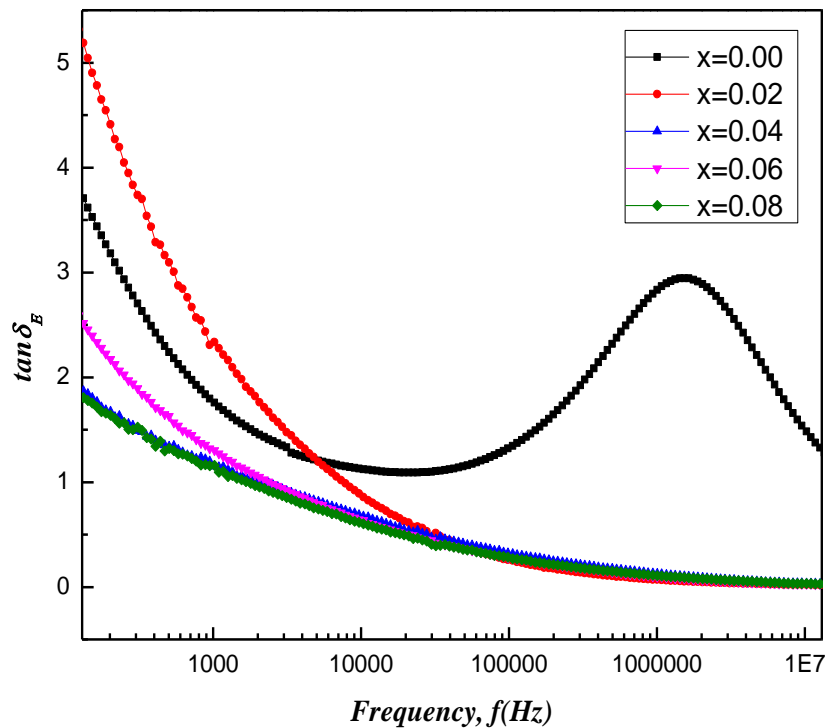
Figure 4.16:   Frequency dependent dielectric loss of $Ni_{0.25}Zn_{0.75}Y_xFe_{2-x}O_4$, [Where x=0.00, 0.02, 0.04, 0.06 and 0.08] ferrites sintered at 1150°C/3 hours.

Figure 4.16 shows the variation of $\tan\delta_E$ with frequency for ferrites at room temperature. The values of loss tangent decreases with increasing Y content in $Ni_{0.25}Zn_{0.75}Y_xFe_{2-x}O_4$ ferrites. The variation of $\tan\delta_E$ with respect to frequency can be explained by two mechanisms: electron hopping and charge defect dipoles. The formation of dipoles contributes to loss tangent in the low frequency range and defect dipoles are responsible at high frequency range in ferrites are formed due to exchange Fe^{3+}- Fe^{2+} exchange, during sintering process. In the low frequency region ferrite contains high resistivity, then grain boundary requires more energy to exchange electron between Fe^{2+}-Fe^{3+} ions. For this reason the energy loss factor, $\tan\delta_E$ is high in the low frequency range. Similar behavior has been observed in the $\tan\delta_E$ vs frequency for ferrite composite by [Slatineanua *et al.,* 2013].

4.5 Effect of Yttrium Substitution on DC Resistivity

Resistivity is an important electrical property of ferrite materials. The electrical properties of ferrite materials depend upon the method of preparation, chemical composition, grain size and sintering temperature. The variation of DC resaistivity as a function of Y content in Ni-Zn ferrites shows Figure 4.17.
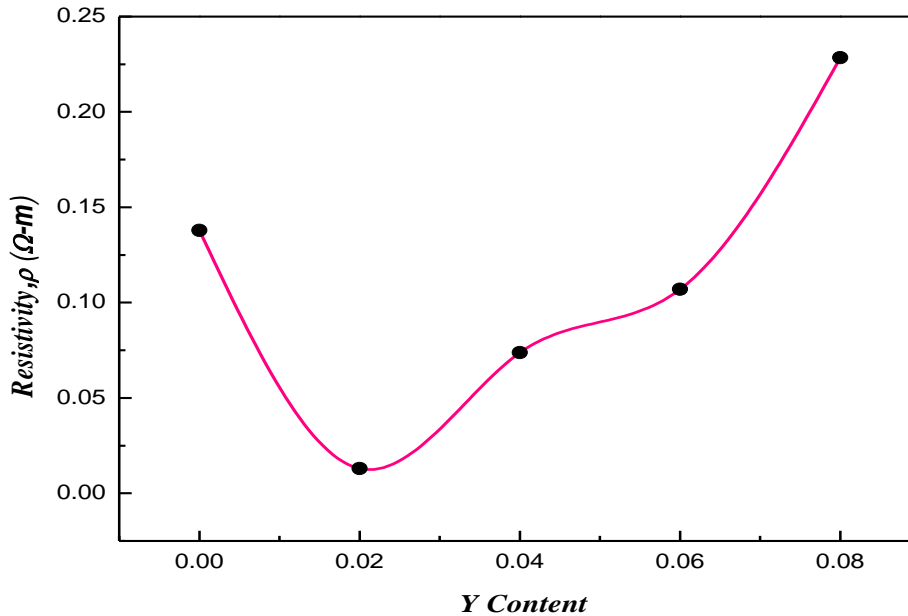
Figure 4.17:   Variation of DC resistivity with Y content in $Ni_{0.25}Zn_{0.75}Y_xFe_{2-x}O_4$ ferrites.

Figure shows electrical DC resistivity of the ferrite increases with increase in Y content except to the sample for x = 0.00 for this reason higher resistivity compared to doped sample. It decreases with the increasing of Y contents for x = 0.02 may be due to the decreases in grain size. Undoped sample is larger grains result in less number of grain boundaries which play as scattering centre for the flow of electrons and therefore decrease of resistivity as doped Y content in Ni-Zn ferrites. From figure shows doped sample in Ni-Zn-Y ferrites can see that Dc resistivity increases with increasing Y content. These $Ni_{0.25}Zn_{0.75}Y_xFe_{2-x}O_4$ ferrites without Y content, Fe concentration is maximum at B-site, when the Y content increased in A-site, a decrease of Fe ion observed in B-site. Here some Fe ion migrated from A to B site to accommodate the increased number of Y ions at A-sites. This means reason electron hopping between Fe and Fe is greater at B-site consequently Fe ions lowers the conduction and subsequently an increase in DC resistivity.

CHAPTER V

CONCLUSIONS

CONCLUSIONS

5.1 Conclusions

The present research work were undertaken mainly investigate of the structural, magnetic and transport properties of polycrystalline $Ni_{0.25}Zn_{0.75}Y_xFe_{2-x}O_4$ [Where x=0.00, 0.02, 0.04, 0.06 and 0.08] are successfully made by the double sintering standard solid state reaction method. The powder samples were presintered at 850°C and pallet and ring shaped samples were sintered at 1150°C. Different measurements of the prepared samples were carried out and results were analyzed carefully to visualize the changes structural, magnetic and some transport properties. Powdered samples were used in XRD, pallet were used for dielectric measurement, resistivity measurement and SEM analysis. Ring shaped sample were used for permeability and magnetization measurements.

From the systematic investigation on the crystallization, magnetic, dielectric and electrical properties the following conclusions:

(i) The XRD patterns confirm that all the $Ni_{0.25}Zn_{0.75}Y_xFe_{2-x}O_4$ [x = 0.00, 0.02, 0.04 and 0.06] samples are of single phase cubic spinel structure without any impurity peaks but x = 0.08 rare earth Y substitution for Fe in ferrite produced secondary phase $YFeO_3$ is puriephasic (Cubic and orthorhombic).

(ii) The lattice constant of $Ni_{0.25}Zn_{0.75}Y_xFe_{2-x}O_4$ increases linearly with increasing in Y content, obeying the Vegard's law.

(iii) The bulk density is lower than the actual X-ray density of the sample. The bulk density decreases with increasing rare earth ion Y^{3+} and the X-ray density increases with increasing x-content. The porosity of the samples increases for x = 0.02 then decreasing for Y content and then again increasing, whereas porosity follows the opposite trend with bulk density. Difficult to remove these closed porosities completely due to the evaporation of constituents specially Zn.

(iv) SEM images showed that Y^{3+} had a significant effect on the grain growth of the sample and the grain size increased with increases Y content but x = 0.08 of $Ni_{0.25}Zn_{0.75}Y_xFe_{2-x}O_4$ ferrites. The grain size of matrix phase is maximum at 1943nm for x = 0.06. Relatively lower grain size of ferrite matrix at x = 0.00 composition

shows other doped Y might be due to the grain growth inhibition caused by $YFeO_3$ are clear visible. Average grain size is estimated in the range from 1355nm to 1877 nm.

(v) The magnetization measurements were carried out by VSM. The value of Saturation magnetization has found to be decreases with the increasing of Y^{3+} doped content for measurable all samples. It can be seen here conventionally that, doping accompanies grain growth and that is responsible for the decreases of magnetization due to the decrease of Fe content. The decrease in M_s can be explained by the cation distribution in which Y^{3+} ions can convert some of Fe^{2+} to Fe^{3+} in B-sites.

(vi) The hysteresis loops do not show any noticeable hysteresis effect. All samples exhibited low coercivity in the range of 25 to 45Oe values indicating that all the samples belong to the family of soft ferrites. Coercivity was also decreased with increasing Y content. The values of the variation of remanent ratio (M_r/M_s) and Y content increased with increasing Y^{3+}content. The variation of coercivity (H_c) and Y content decreased with increasing Y^{3+} content, which follows the opposite trend with the variation of remanent ratio and Y content.

(vii) Frequency dependent initial permeability remains almost constant until very high frequency up to 60 MHz and then drops rapidly. It is seen that real part of initial permeability (μ') remains almost constant until very high frequency (around 60MHz) and then drops rapidly. The fairly constant μ' values over a wide range of frequency region are known as the zone of utility because it demonstrates the compositional stability and quality of the prepared samples. Here the initial permeability remains stable for a long frequency range due to hopping of electron between Fe^{2+} and Fe^{3+}. The initial permeability is slightly decreases with increasing Y content whereas magnetic loss in association with loss tangent decreases.

(viii) The frequency dependent imaginary permeability initially high at low frequency zone for all the samples and then decreases with increasing frequency almost constant high frequency range. At high frequencies at constant μ'' parameters become more

significant, during grain growth pores become fewer, which act as independents to domain wall motion due to pinning wall.

(ix) The dielectric dispersion is rapid decreases at lower frequency region and it remains almost independent at high frequency side. The effect Y^{3+} ion into Ni-Zn ferrite has no pronounced effect of high frequency region but significantly decreases the dielectric constant in the low frequency region. The effect of rare earth Y^{3+} substitution into into Ni-Zn ferrite has no pronounced effect on the dielectric constant in high frequency, but significantly decreases the dielectric constant in the low frequency range. The dielectric behavior of ferrites may be explained on the basis of the mechanism of the dielectric polarization process and is similar to that of the conduction process.

(x) DC resistivity increases with increasing Y content in Ni-Zn ferrites. Basically Fe ion lowers the conduction and subsequently an increase in resistivity.

5.2   Scope for Future Work

Some studies on different aspects are possible for fundamental interest and also for potential applications of the studied materials. The following experiment and activities would be obtained as future work as the extension of this research.

- The characteristics in crystallization formation will be achieved by DSC thermal analysis.
- Neutron diffraction analysis may be performed for these compositions to determine the distribution of substituted ions between A and B sites. Mössbauer spectroscopy can also be studied.
- The bond length and bonding mechanism would be carried out by FTIR spectroscopy.
- Some AC and DC electrical properties may be studied.
- SEM can be studied for better understand surface nature and domain wall motion with substitution rear earth in ferrites shows biphasic microstructure constituted of matrix of dark grains and a second orthoferrite phase.

REFERENCES

REFERENCE

Alex Goldman 1990: Modern Ferrite Technology, Van Nosttrand Reinhold, New York, p-71.

Abdeen A. M. 1998: Electrical conduction in Ni-Zn ferrites; J. Magn. Magn. Mater., 185, 199.

Ahmed M. A., Okasha N. and Salah L. 2003: Influence of Yttrium ions on the magnetic properties of Ni-Zn ferrites; J. Magn. Magn. Mater, Vol. 264, Nos. 2 - 3, pp. 241-250.

Ahmed M. A., Oskasha N. and Sayed M. M. EI. 2017: Enhancement of the physical properties of rare earth substituted Mn-Zn ferrites prepared by flash method; Ceramics International 33.1: 49-58.

Bharathi K. K., Chelvane J. A., Markandeyulu G.2009: Magnetoelectric properties of Gd and Nd-doped nickel ferrite; J. Magn. Magn. Mater. 321: 3677–3680.

Buschow K. H. J. and De Boer F. R. 2004: Physics of Magnetism and Magnetic Materials; Kluwer Academic Publishers, New York, USA.

Craik D. J. 1975: Magnetic Oxide; Part 1, John Wiley & Sons, Bristol, ch. 9, part-2.

Cullity B. D. 1972: Introduction to Magnetic Materials, Addison - Wisley Publishing Company, Inc.,California.

Dai H., Li T.; Xue R.; Chen Z. 2012: Effects of Europium Substitution on the Microstructure and electric Properties of Bismuth Ferrite Ceramics; J. Superconductor. Nov. Magn. 25: 109-1154.

Forner S. 1959: Versatile and sensitive Vibrating Sample Magnetometer; Rev. Sci. Instr. 30, P.548.

Fujimoto M. 1994: J. Am. Ceram. Soc. 77 (11), 2873.

Globus A., Duplex P. Guyot M. 1971: Determination of initial magnetization curve from crystallites size and effectively anisotropy field; IEEE Trans. Magn., Vol. 7, 3, 617 – 622.

Goldman A. 1999: Handbook of Modern Ferromagnetic Materials; Kulwer Acad. Pub, Boston, U.S.A.

Globus A., Pascard H. and Cagan V. 1977: Distance between magnetic ions and fundamental properties in ferrites; Le Journal de Physique Colloques 38, C1-163.

Guo D., Fan X., Chai G., Jians C., Lix. and Xue D. 2010: Structural and Magnetic Properties of Ni-Zn Ferrite Films with High Saturation Magnetization Deposited by Magnetron Sputtering; Appl. Surf. Sci., 256, 2319 - 2332.

Guo L., Shen X., Meng X., Feng Y. 2010: Effect of Sm^{3+} ions doping on structure and magnetic properties of nanocrystalline $NiFe_2O_4$ fibers; J. Alloy. Compd. 490 : 301–306.

Gupta T. K. and Coble R. L. 1968: Sintering of ZnO: I, Densification and Grain Growth; J. Am. Ceram. Soc., Vol. 51, pp. 521 – 525.

Herzer G., Venqnez M., Krobel M., Zhokov A. Reininser T. and Davies H. A. 2005: Present and Future Application of Nanocrystalline Magnetic Materials; J. Magn. Magn. Mater, 294, 252.

Haque M. M., Huq M. and Halcim M. A. 2008: Influence of CuO and sintering temperature on the microstructure and magnetic properties of Mg-Cu-Zn ferrites; J. Magn. Magn. Mater., Vol. 320, 2792 – 2799.

Haque M. M., Huq M. and Halcim M. A. 2009: Densification, magnetic and dielectric behavior of Cu-substituted Mg-Zn ferrites; Mat. CHEM., phys., Vol. 112, 580 – 586.

Haque M. M., Huq M. and Halcim M. A. 2009: Effect of Zn^{2+} Substitution on the Magnetic Properties of $Mg_{1-x}Zn_x Fe_2O_4$ Ferrites, Physica, B404, 3915.

Hossain A. K. M. A. 1998: Investigation of colossal magnetoresistance in bulk and thick film magnetites; Ph. D. Thesis, Imperial College, London.

Hossain M. A. January -2017: Effect of Rare Earth Metal Substitution on the Structural, Magnetic and Transport Properties of Ni-Zn Ferrites; M. Phil. Thesis, KUET, Khulna, Bangladesh

Hossain M. A., Khan M. N. I. and Sikder S. S. 2017: Structural Magnetic and Dielectric Behaviors of Y^{3+} Substituted Ni-Zn Ferrites; Int. J. of Nano Science Trends and Tech. 1.2: 1-19.

Hu Jun and Yan Mi 2005: Preparation of high permeability Ni-Cu-Zn ferrite; J. Zhejiang Univ. SCI B, Vol. 6, 580 – 583.

Kambale R. C., Song K. M., Koo Y. S. and Hur N. 2011: Low temperature synthesis of nanocrystalline Dy^{3+} doped cobalt ferrite: Structural and magnetic properties; J. Appl. Phys. 110: 053910.

Khan Z. H. , Mahbubur Rahman M., Sikder S. S. , Hakim M. A., Shireen Akhter, Das H. N. and Anjuman B. 2013: Thermal Hysteresis of Cu Substituted $Ni_{0.28}Cu_{0.10+x}Zn_{0.62-x}Fe_{1.98}O_4$ Ferrites; Advanced Chemistry Letters, 2, 1 - 6.

Khan Z. H. , Mahbubur Rahman M., Sikder S. S. , Hakim M. A. and Saha D. K. 2013: Complex Permeability of Fe-deficient Ni-Cu-Zn Ferrites; Journal of Alloys and Compounds, 548, 208 – 215.

Kigery W. D., Bowen H. K. and Uhlmann D. R. 1975: Introduction of Ceramics, New York, John Wiley and Sons.

Kittel C. 1996; Introduction to Solid State Physics; 7th edition, John Wiley & Sons, Inc., Singapore.

Kodama R. H. 1999: Magnetic nanoparticles; J. Magn. Magn. Mater. Vol. 200, 359 - 372.

Kolekar C. B., Kamble P. N., Vaingankar A. S. 1995: Thermoelectric Power in Gd^{3+} substituted Cu-Cd Ferrites; J. Bull. Mater. Sci. 18(2), 133.

Jacob B. P., Thankachan S., Xavier S., Mohammed E. M. 2011: Effect of Gd^{3+} doping on the structural and magnetic properties of nanocrystalline Ni–Cd mixed ferrite; Physica Scripta 84 : 045702.

Jacobo S. E., Uhalde S. D., Bertorello H. R. 2004: Rare Earth influence on the structural andmagnetic properties of Ni-Zn ferrites; *J. Magn. Magn. Mater.* 272: 2253 - 2254.

Jadhav S. R., Sawant S. S. and Patil S. A. 1999: Tempaerature and frequency dependence of initial permeability in Zr^{4+}substituted Cu-Zn ferrites; J. less-common Met., Vol. 158,199 - 20.

Jie S., Lixi W., Naicen X., Qitu Z. 2010: Introduction to Ferrite; J. Rarte Earths, 28, 445.

Jing J., Liang-Chao L., Feng X. 2006: Preparation, Characterization and Magnetic Properties of PAN/La-substituted LINi Ferrite Nanocomposites; Chin. J. Chem., 24, 1804.

Jing J., Liang-Chao L., Feng X. 2007: Structural Analysis and Magnetic Properties of Gd-Doped Li-ni Ferrites Prepared Using Rheological Phase Reaction Method; J. Rare Earths 25, 79.

Jonker G. H. 1959: Analysis of the semiconducting properties of cobalt ferrite; J. Phys. Chem. Solids, 9(2), 165-175.

Lange F. F. 1989: Thermodynamics of densification: II, grain growth in porous compacts and relation to densification; J. Am. Ceram. Soc., Vol. 72, pp. 735 – 741.

Li L., Tu X., Peng L., Zhu X., 2012: Structure and Static Magnetic Properties of Zn-substitute Ni-Zn Ferrites Thin Synthesis by Sol-gel Method; J. Alloys Comp. 545, pp. 67 – 69.

Lu X., Liang G., Sun Q. and Yang C. 2011: An Interdisciplinary Journal devoted to Rapid Communications on the Science, Applications and Processing of Materials; Matter. Lett., 65, 674 – 676.

Maxwell J. 1873: Electricity and Magnetism; Vol.1 Oxford University Press. London Wanger K. 1913: Ann. Phys. 40, 817.

Mendelson, M. I. 1969: Average Grain Size in Polycrystalline Ceramics; J. Am. Ceram, Soc. 52, 8,443 - 446.

Mondal P. K. May-2018: Study of the Effect of Rare Earth Ions on the Structural, Magnetic and Electrical Properties of Cu-Zn Ferrites; M. Sc. Thesis, KUET, Khulna, Bangladesh

Nakamura T. 1997: Low Temperature Sintering of Ni – Cu- Zn ferrite and its Permeability Spectra", J. Magn. Magn. Mater., 168 , 285 – 291.

Nakamura T., Tsutaka T., Hatake Yana K. 1994: Frequency dispersion of permeability in ferrite composite materials", J. Magn. Magn. Mater, 138 319.

Naughton T. B. and Clark R. D. 2007: Lattice Expansion and Saturation Magnetization of Nickel –Zinc Ferrite Nanoparticles Prepared by Aqueous Precipitation; Am, Ceram., Soc., 90, 3541 - 3546.

Néel L. 1948: Propriétées magnétiques des ferrites; Férrimagnétisme et antiferromagnétisme, Annales de Physique (Paris) 3, 137–198.

Nelson J. B., Riley D. P. 1945: An experimental investigation of extrapolation methods in the derivation of accurate unit-cell dimensions of crystals; Proc. Phys. Soc. London 57, 160.

Nikumbh A. K., Pawar R. A., Nighot D. V., Gugale G. S., Sangale M. D., Khanvilkar M. B., Nagawade A.V. 2014: Structural, electrical, magnetic and dielectric properties of rare-earth substituted cobalt ferrites nanoparticles synthesized by the co-precipitation method; J. Magn. Magn. Mater. 355 : 201–209.

Paulus M., Edited by H. Palmour, Davis R. F. and Hare T. M. 1978: Ceramics Materials Science Research. II; Plenum Press, New Work.

Peng J., Hojamberdiev M., Xu Y., Cao B., Wang J., Wu H. 2011: Hydrothermal synthesis and magnetic properties of gadolinium-doped $CoFe_2O_4$ nanoparticles; J. Magn. Magn. Mater. 323: 133–137.

Rare Earth Elements - Critical Resources for High Technology: United States Geological Survey, Fact Sheet 087-02.

Rezlescu E., Rezlescu N., Popa P. D., Reslescu L. and Pasnicu C. 1997: The Influence of R_2O_4 (R = Yb, Er, Dy, Tb, Gd, Sm and Ce) on the Electric and Mechanical Properties of a Nickel-Zinc Ferrite; Physica(a). Status Solidi, A 162, 673 – 678.

Rezlescu N., Rezlescu E., Pasnicu C., Craus M. L. 1994: Effect of the Rare Earth Metal of Some Properties of a Nickel-Zinc Ferrite; J. Phys Condensed Matter. 6 : 5707.

Shah M. A. 1971: Electricity and Magnetism; Sh. Ghulam Ali and Sons (Publisher) lid., Lahore, Pakistan.

Slatineanua T., Iordana A. R., Oanceaa V., Palamarua M. N., Dumitrub I., Constantinb C. P., Caltunb O. F. 2013: Magnetic and dielectric properties of Co–Zn ferrite; Materials Science and Engineering B. 133, 84: 1-8.

Smit J. and Wijin H. P. J. 1959: Ferrites; Philips Technical Libery C Wiley, New York.

Snelling E. C. 1988: Soft Ferrites; Properties and Applications, Butter-worth and Co. (Publishers) Ltd., London.

Spaldin N. A. 2003: Magnetic Materials; Fundamentals and device applications, Cambridge University Press.

Spladin and Nicola A. 2010: " Ferrimagnetism". Magnetic materials: fundamentals and (2nd ed.). Cambridge: Cambridge University Press. pp. 113& ndash, 129. ISBN 9780521886697

Standley K. J. 1972: "Oxide Magnetic Materials; 2 ed., Oxford University Press.

Sun G., Li J., Sun J. and Yang X. 2004: The Influences of Zn^{2+} and some Rare Earth Ions on Magnetic Properties of Ni-Zn Ferrites; J. Magn. Magn. Mater., 281, 173 – 177.

Tahir Abbas, Islam M. U. and Ashraf Ch M. 1995: Study of Sintering Behavior and Electrical Properties of Cu-Zn-Fe-O System; Mod. Phy. Letts., B 9(22), 1419.

Tsay C. Y., Liu K. S., Lin T. F. and Lin I. N. 2000: Microwave Sintering of NiCuZn Ferrites and Multilayer Chip Inductors; Journal of Magnetism Materials, Vol. 209, pp. 189 – 192.

Tsutaoka T., Ueshima M., Tokunga T., Nakamura T., Hatakeyama K. 1995: Frequency dispersion and temperature variation of complex permeability of Ni-Zn ferrite composite materials; J. Appl. PHYS., Vo. 78, 6, 3983 – 3991.

Vegard's L. 1921: Die constitution der mischkristalle und die raumfullung der atome; Z. Phys. 5, 17.

Van Vleck 1989: Elements of Material Science and Engineering; 6th Ed., Addison Wesley Co. (Publisher) Ltd., New York.

Valenzuela R., 1994: Magnetic Ceramics; Cambridge University Press, Cambridge.

Vanuitert L. G. 1955: High Resistivity Nickel Ferrites – the Effect of Minor Additions of Maganese or Cobalt; J. Chemi. Phys. 23, 1883.

Verma A., Goel T. C., Mendritta R. G., Alam M. I. 1990: Dielectric properties of Ni-Zn ferrites prepared by the citrate precursor method; Mater. Sci. Eng. 60, 156 – 162.

Verway E. J. W. , Heilmann E. L. J. and Romeijin F. C. 1947: Physical Properties and Cation Arrangement of Oxides with Spinel Structure 11. Electronic Conductivity; J. Chem. Phys. 15 (4): 181 - 187.

Valenzuela R.1994: Magnetic Ceramics; Cambridge University Press., Cambridge.

Von Aulock W. H. 1965: Hand Book of Microwave Ferrite Materials; Academic Press, New York, London.

Yan M. F. and Johnson D. W. 1978: Impurity induced exaggerated grain growth in Mn-Zn ferrites; J. Am. Ceram. Soc., 61, 342.

Yang Z. H., Gong Z., Q., Li H. X., Ma Y. T. and Yang Y. F. 2006: Synthesis of Ni-Zn Ferrites and Its Microstructure and Magnetic Properties; Journal of Central South University of Technology, 13, 618-623.

Wohlfarth E. P. 1980: A handbook on the properties of magnetically ordered substances; Elsevier Science B. V., The Netherland.

Zhenxing Yue, Zhou Ji, Longtu Li, Xiaolui Wang and Zhilun Gui 2001: Effect of copper on the electromagnetic properties of Mg-Zn-Cu ferrites prepared by Sol-gel auto-combustion method; Mater. Sci. Eng. B 86, 64.

CONFERENCE PUBLICATIONS

1. **S. Akther**, M. A. Hossain, M. N. I. Khan and S. S. Sikder; "Investegation of the Magnetic Properties of Yttrium Substituted Ni-Zn Ferrites for the Use of Core Magnetic Materials of Inductor", International Conference on Physics 2018, 08-10 March, DU, Dhaka-1000, Bangladesh.

2. **S. Akther**, M. A. Hossain, M. N. I. Khan and S. S. Sikder; "Effect of the Yttrium (Y) Substitution on on Magnetic and Transport Properties in Ni-Zn Rare Earth Ferrites"; Conference on Weather Forecasting and Advances in Physics, 11-12 May, 2018, KUET, Khulna-9203, Bangladesh.